# DIPLOMARBEIT
## Master's Thesis

## A new nanoindentation protocol for identifying the elasticity of undamaged extracellular bone tissue

ausgeführt zum Zwecke der Erlangung des akademischen Grades
eines Diplom-Ingenieurs/ einer Diplom-Ingenieurin

unter der Leitung von

Univ. -Prof. Dipl.-Ing. Dr. techn. Christian Hellmich
Dipl. -Ing. Maria-Ioana Pastrama
und
Dipl. -Ing. Hawraa Kariem

Inst.Nr.: E202

Institut für Mechanik der Werkstoffe und Strukturen

eingereicht an der Technischen Universität Wien
Fakultät für Bauingenieurwesen

von

Irina Furin

Matr.Nr.: 1129721

Rauchenwarther str. 70.
A-2320 Rauchenwarth

Wien, am 20.10.2015

1

# Abstract

For the determination of the Young's modulus of bone tissues several methods are widely in use, among them quasi-static mechanical tests, ultrasound tests, and nanoindentation tests. However, the key question of how an elastic modulus can be reliably retrieved from such tests, is surprisingly unsettled. In this Master's thesis, a new method for determination of the elastic modulus of extracellular bone matrix from very many nanoindentation results is developed, based on an earlier contribution in the field of brittle ceramics used in bone tissue engineering (Kariem et al., 2015).

576 nanoindentation tests were performed on carefully polished bovine femoral bone samples, and the results were statistically analyzed,by fitting a number of Gaussian distribution functions to the histogram made up by all indent-specific elastic moduli, each of them being retrieved from Oliver and Pharr's solution for the elastic half space. The fitting procedure was based on an evolutionary algorithm (Weicker, 2007; Jaindl et al., 2009), and revealed the existence of several material phases with distinct expected values for their corresponding elastic moduli, according to the premises of the statistical or grid nanoindentation technique (Ulm et al, 2007). The stiffest of these moduli refers to the undamaged elastic modulus of extracellular bone tissue, while all other moduli reflect influences of microcracks in the vicinity of the indent, or directly branching off from the microcracks; this was explicitly confirmed by a preliminary nanoindentation test series performed under a Scanning electron microscope (SEM).

The value obtained with our new method for the undamaged extracellular femoral bovine bone matrix, amounting to 31.4±2.5 GPa, appears remarkably well to the results obtained from unloading quasi-static compression tests on single-micro-sized micropillars which were SEM-FIB-milled from the same type of bone (Luczynski et al., 2015); and to predictions of a carefully validated micromechanical model for bone (Morin and Hellmich, 2014).


This is regarded as major step toward reliable determination of the elastic properties of bone at a scale, where „universal" composition and elasticity laws can be retrieved (Vuong and Hellmich, 2011); and hence, to drive forward bone mechanics to a level which would finally allow for predictive fracture risk assessment in biomedicine up to the level which have been reached in traditional civil or mechanical engineering, and for advanced, computer-aided design of materials for bone replacement.

# Table of contents

# 1. Introduction

The idea of developing and implementing a fundamentally new evaluation protocol for nanoindentation measurements originated in the fact that this mechanical testing method is used to measure the load and displacement behavior of materials with very different types of structure and parameters. According to our observed measurements, the Young modulus of elasticity obtained from nanoindentation tests shows a relatively wide range of results, depending on the indentation location - especially in brittle or porous materials. This can easily also be concluded from literature, as many studies report very different values for the Young modulus from nanoindentation for one and the same material.

This led us to the theory that the results of nanoindentation tests could be affected by fine, visually not detectable cracks, i.e. a damage of the material could occur. This damage could be a result of sample preparation, as well as a consequence of the nanoindentation procedure itself. Usual evaluation methods only filter out the most evident measurement failures or incorrect data, but none of them takes into account possible material damage. The results are usually fitted with one distribution, or an average of more measurements is calculated, which may also include results for damaged material; this is the reason why nanoindentation tests usually deliver a lower Young's modulus than quasi-static mechanical or ultrasonic tests.

This Master's Thesis is focused on determining the exact Young's modulus of pure, non-damaged bovine cortical bone. The description of the method and the results, which have been put together in a paper that builds the core of this thesis (and has been submitted to the *Journal of the Mechanical Behavior of Biomedical Materials*), describes how the Young modulus of the undamaged material phase was extracted. For this we performed 576 nanoindentation tests on finely polished samples obtained from an 18-month-old bovine femur bone, and developed an evaluation method which excludes damaged material phases with high certainty. This was achieved by fitting a different number of cumulative distributions (in our case from 1 to 10) - i.e. different distribution groups - to the measurement data with the help of the evolution strategy. This strategy iteratively changes the normal cumulative distribution functions and their weights, until their summarized combination best fits the original data.

The optimal number of distributions for fitting our experimental nanoindentation results was chosen to be that for which the relative error to the original data was minimal. Within this group, the very last distribution corresponded to the intact material, its mean representing the Young modulus of pure, non-damaged bovine cortical bone – while all other distributions were considered to represent several damaged material phases. The results obtained with this

protocol were compared with those previously obtained from micropillar compression tests, and the agreement was very good.

At the end of this thesis, a short future outlook is offered, presenting further possibilities for proving the existence of damage that could affect the results of nanoindentation tests.

2. **Paper entitled "A new nanoindentation protocol for identifying the elasticity of undamaged extracellular bone tissue"**

# A new nanoindentation protocol for identifying the elasticity of undamaged extracellular bone tissue

Irina Furin, Maria-Ioana Pastrama, Hawraa Kariem, Krzysztof W. Luczynski, Olaf Lahayne, Christian Hellmich[1]

*Institute for Mechanics of Materials and Structures, Vienna University of Technology (TU Wien), Austria*

## Abstract

We here describe a new method for nanoindentation-based identification of the undamaged extracellular bone matrix. The underlying premise is that the tested bovine bone sample is either initially damaged (i.e. shows some microcracks) or that the nanoindentation process induces such microcracks, or both. Then, hundreds of indentations may partially relate to an intact material phase (sufficiently far away from microcracks), and partially relate to differently strongly damaged material phases. Corresponding elastic phases properties are identified from the statistical evaluation of the measured indentation moduli, through representation of their histogram as a weighted sum of Gaussian distribution functions. The resulting undamaged elastic modulus of bovine femoral extracellular bone matrix amounts to 31 GPa, a value agreeing strikingly well with both direct quasi-static modulus tests performed on SEM-FIB-produced micropillars (Luczynski et al, 2015), and with the predictions of a widely validated micromechanics model (Morin and Hellmich, 2014). Further confidence is gained through observing typical indentation imprints under an SEM, indeed confirming the above stated premise on the types of microcracks present on the tested bone surface.

**Keywords:** statistical nanoindentation, bovine bone, micromechanics, elastic modulus, evolutionary strategy

---

[1] Corresponding author
*E-mail address*: christian.hellmich@tuwien.ac.at (Christian Hellmich)

## List of symbols

| | |
|---|---|
| $A$ | projected area of the elastic indentation contact |
| $\mathbb{C}_{excel}$ | stiffness matrix of the extracellular bone matrix |
| $\mathbb{C}_{excel}^{-1}$ | inverse of the extracellular bone stiffness matrix |
| $D_{excel,iijj}$ | component of the extracellular compliance tensor |
| $D^{exp}$ | experimental cumulative distribution function (CDF) of the measured data |
| $D^{model}$ | weighted sum of the Gaussian cumulative distribution function |
| $D_j^{model}$ | Gaussian model cumulative distribution function for material phase $j$ |
| $\mathbb{D}_{excel}$ | extracellular compliance tensor |
| $e_{rel}$ | relative error |
| $E_t$ | elastic modulus of the indentor tip |
| $E_r$ | reduced elastic modulus |
| $E_s$ | elastic modulus of the extracellular bone matrix |
| $E_{s,i}$ | i$^{th}$ experimental value of $E_s$, as determined by nanoindentation |
| $E_{BT}$ | elastic modulus of undamaged, intact extracellular bone tissue material |
| $f_j$ | weighting factor of the Gaussian cumulative distribution function related to material phase $j$ |
| $i$ | indexing the number of indentations $i \in [1, N]$ |
| $k$ | number of mutation cycles |
| $N$ | total number of indentations |
| $o$ | optimal number of Gaussian cumulative distribution functions |
| P | number of pixels in each scan edge |
| $R^2$ | coefficient of determination |
| $R_q$ | root-mean-squared average roughness (RMS) of the topography of the surface |
| $S$ | stiffness |
| $u$ | variable of the normal distribution function |
| $z_{ij}$ | measured height at position ($i$,$j$) from the mean plane |
| $\mathcal{E}$ | sum of squares of residuals |
| $\mu_j$ | mean value related to material phase $j$ |
| $\nu_t$ | Poisson's ratio of the indentor tip |
| $\nu_s$ | Poisson's ratio of solid bone matrix |
| $\sigma_j$ | standard deviation related to material phase $j$ |
| $\tau_{relax}$ | characteristic time of relaxation |
| $\dot{p}_{relax}(t)$ | dependence of the holding portion of the load data on time |

# 1 <u>Introduction</u>

Ever since the famous paper of Oliver and Pharr (1992), indentation techniques have regained a very prominent role in material characterization, by extending their application to get smaller and smaller scales, and coining a new term for these developments: nanoindentation. Originally applied to materials such as fused silica, soda–lime glass, and single crystals of aluminum, tungsten, quartz, and sapphire, the method was, soon thereafter, extended to biological materials such as bone (Rho et al., 1997; Rho and Roy, 1999; Zysset et al., 1999; Hengsberger and Zysset, 2002; Rho and Zioupos, 2002). These applications were motivated, according to Rho et al. (1997), by the wish to measure the "intrinsic" elastic properties of several of the microstructural components of bone. In this context, „intrinsic" refers to the properties of bone tissue or extracellular bone matrix defined at the scale of several to several tens of micrometers, rather than to those of a macroscopic (typically millimeter-sized) sample of cortical or trabecular bone. The aforementioned references revealed important new insight into these "intrinsic" bone properties. On the one hand, this insight concerned heterogeneity of bone tissue properties at different (small) observation scales; e.g. it was found that the bone tissue elastic properties of vertebrae are much smaller than those of tibiae (Rho et al., 1997); that tibial osteonal regions are softer than interstitial ones (Rho et al., 1997); and that human femoral trabecular bone tissue is softer than cortical bone tissue (Zysset et al., 1999). On the other hand, such tests revealed that bone tissue properties are, on average, *independent* of adult tissue age (Hoffler et al., 2000; Rho et al., 2002; Feng and Jasiuk, 2010; Wolfram et al., 2010).

Hence, while the method was very successful in terms of evidencing local differences (exactly as the pioneers of the method had actually hoped for), the reconciliation of the quantitative values it provided, with those of other methods delivering elastic properties, such as ultrasonic and quasi-static mechanical testing, turned out as challenging: In more detail, applying ultrasonic signals in the MHz frequency regime to bone samples, as reported by Ashman et al. (1984), Lees et al. (1979), and Lees and Ahern (1983), results in the propagation of waves the wavelengths of which are typically less than one millimeter; and according to the separation of scales principle in continuum (micro-)mechanics (Zaoui, 2002; Drugan and Willis, 1996) and the continuum theory of elastic waves (Fedorov, 1968), the aforementioned wavelengths need to be much larger than the characteristic material volume (also called representative volume element) whose elastic properties are characterized by the ultrasonic waves (Kohlhauser and Hellmich, 2013). Accordingly, MHz-regime-related ultrasonic tests reveal the elastic properties at the bone tissue scale (i.e. that of a material volume with several

microns characteristic length), averaged over the size of the ultrasonically tested sample (Fritsch and Hellmich, 2007; Vuong and Hellmich, 2011).

However, such ultrasonically determined elastic stiffness values are, as a rule, consistently larger, than those obtained (on average) from nanoindentation campaigns (Malandrino et al., 2012). And the same discrepancy was very recently found in the context of unloading mechanical tests on SEM-FIB-produced micropillars (Luczynski et al., 2015), again delivering results in line with ultrasonic tests, but stiffer than those obtained from nanoindentation.

This discrepancy motivates the present study, aiming at an improved nanoindentation protocol that may indeed deliver results, which are consistent with the aforementioned well-established and well-understood methods for elasticity determination, namely ultrasonics tests and unloading mechanical tests. Our proposition is that the aforementioned discrepancy may stem from bone microcracks measuring several to several tens of micrometers (Schaffler et al., 1994; Wenzel et al., 1996; O'Brien et al., 2000; Chapurlat et al., 2007), which may be - to some extent - initially present close to the indentation sites, but may be also actively induced by the indentation process itself. The basis for this proposition is that bone tissue is known to behave plastically at the level of several microns, as revealed by nanoindentation test imprints studied in the context of plasticity theory for nanogranular materials (Tai et al., 2006), by advanced micromechanics theories validated through various biochemical and biomechanical experiments (Fritsch et al., 2009), and by mechanical tests of single micrometer-sized micropillars (Luczynski et al., 2015; Schwiedrzik et al., 2014); while it shows a quasi-brittle behaviour at the scale of tens to hundreds of micrometers (Ritchie, 2011).

Accordingly, we here target at distinguishing between tests conducted sufficiently far from microcracks *and* not inducing any neighbouring cracking events, from tests conducted in the absence of such events, and hence fulfilling more appropriately the conditions needed for nanoindentation evaluation as proposed by Oliver and Pharr in 1992. Therefore, we take inspiration from the so-called statistical or grid nanoindentation technique developed in the late 2000s (Constantinides and Ulm, 2007; Ulm et al., 2007; Vandamme and Ulm, 2009), where a statistical evaluation of very many indentation results allows for assignment of subgroups of these results, to different chemical material phases present in a highly micro-heterogeneous material; and basically extend this idea from purely chemical differences between phases, to different degrees of mechanical *damage* present in the phases, or in other

words, to indents differently close to crack-type defects. Thereby, our interest focusses exclusively on the one undamaged phase, and its elastic properties.

The corresponding experimental and data evaluation steps are given in greater detail in Section 2, and the corresponding results for the elasticity of the undamaged phase are then compared to tests giving direct access to this elasticity, namely to micropillar tests, and to ultrasonic tests in combination with advanced micromechanical theories (Morin and Hellmich, 2014). This comparison is further discussed in Section 4, which concludes the paper.

## 2  <u>Materials and Methods</u>

### 2.1  Sample preparation

A diamond saw (Isomet, Buehler, USA) was used to cut, under constant distilled water irrigation, four plane-parallel cortical bone samples with a thickness of 3.5 mm, and measuring roughly 10 times 12 mm in the two other directions, from an 18-month old bovine femur, normal to the longitudinal bone axis. The samples then underwent a number of preparation steps, between which they were kept in a freezer at -20 degrees C, in order to preserve their mechanical properties (Fölsch et al., 2011; Nazarian et al., 2009; Linde & Sørensen, 1993). As a first processing step, the samples were glued onto glass slides and polished with a polishing machine (PM5, Logitech, Scotland), in order to provide flat, i.e. low-roughness, surfaces, as they are needed for meaningful nanoindentation. Thereby, the polishing machine was operated in the "sweeping arm" mode with 10 sweeps/minute. In this mode the polishing paper undergoes a rotating movement only, while the sample holder with the sample is not only rotating, but also translating. In the first polishing step, all four samples were polished with coarse polishing paper (particle size 18.3 μm) for 3 minutes, in order to make sure that the top of the sample is completely parallel to the bottom of sample attached to the glassy specimen holder; this provides an even surface during indentation without any tilt. The 3-minute coarse grinding procedure resulted in a loss of approximately 0.5 mm in thickness for each sample. In the second polishing step the samples were polished with a napped cloth impregnated with 1 μm, high performance, polycrystalline diamond spray (DP-Spray P), for different amounts of time (see Table 1 for details), so as to achieve an even, finely polished surface with a minimized roughness. According to the protocol of Miller et al. (2008), the use of only one size of diamond suspension for the finishing of the sample surface increases the

repeatability of the procedure. A visual comparison of the differently long polished sample surfaces was performed with a microscope (Zeiss Imager Z1m), together with a comparison of the surface roughness, as described in the next section.

Table 1: Polishing protocol for sample preparation

| Sample number | Particle size of sandpaper [µm] | Polishing time [min] | Plate Speed [rpm] |
|---|---|---|---|
| 1 | 18.3 | 3 | 10 |
| | 1 (diamond suspension on a cloth) | 120 | 20 |
| 2 | 18.3 | 3 | 10 |
| | 1 (diamond suspension on a cloth) | 180 | 20 |
| 3 | 18.3 | 3 | 10 |
| | 1 (diamond suspension on a cloth) | 240 | 20 |
| 4 | 18.3 | 3 | 10 |
| | 1 (diamond suspension on a cloth) | 300 | 20 |

## 2.2 Roughness determination

The roughness of Sample 1 (120 minutes of 1 µm polishing) and Sample 4 (300 minutes of 1 µm polishing) was measured using the scanning probe microscopy (SPM) mode of a TriboIndenter system (Hysitron Inc., USA). Two topographic images were made at two different locations using scan sizes of 15×15 µm$^2$. The root-mean-squared average roughness (RMS) of the topography of the surface, $R_q$, was calculated as

$$R_q = \sqrt{\frac{1}{P^2} \sum_{i=1}^{P} \sum_{j=1}^{P} z_{ij}^2} \qquad (1)$$

where P denotes the number of pixels in both scan edges, and $z_{ij}$ is the height at position $(i, j)$ from the mean plane (Miller et al., 2008).

## 2.3 Nanoindentation

In order to check the undamaged elasticity of cortical bovine bone, nanoindentation tests were performed on the four prepared samples, using a Berkovich diamond tip attached to a TriboIndenter nanoindenting system (Hysitron Inc., Minneapolis, MN). Displacement control to a depth of 250 nm with a loading- and unloading rate of 40 nm/s and a holding time of 20 s was used, according to a previously published protocol for bone testing (Reisinger et al., 2011). On each sample a grid of 12x12 indents with 5 µm spacing was defined, resulting

in altogether 576 indentations. The measurements were evaluated according to the method of Oliver and Pharr (1992), which defines the stiffness $S$ as the ratio of load and displacement at the peak load end of the unloading curve,

$$S = \frac{2}{\sqrt{\pi}} E_r \sqrt{A} \tag{2}$$

and introduces the reduced modulus, $E_r$ which considers both the displacement of the sample, $E_s$, as well as that of the Berkovich indenter tip, $E_t$:

$$\frac{1}{E_r} = \frac{(1 - \nu_t{}^2)}{E_t} + \frac{(1 - \nu_s{}^2)}{E_s} \tag{3}$$

with $\nu_s$ and $\nu_t$ as the corresponding Poisson ratios. The elastic modulus of the sample results then from the above equation:

$$E_s = \frac{(1 - \nu_s{}^2)}{\dfrac{1}{E_r} - \dfrac{(1 - \nu_t{}^2)}{E_t}} \tag{4}$$

Determination of $E_s$ according to (4) requires knowledge of Poisson's ratio of extracellular bone matrix, $\nu = 0.3$ (van Rietbergen et al., 1995), as well as of the Poisson ratio and the elastic modulus of the diamond indenter tip, amounting to $\nu_t = 0.07$ and $E_t = 1141$ GPa.

The $N = 576$ test results for the value of the elastic modulus $E_{s,i}$, $i = 1, \dots, N$, were evaluated considering the potential (initial or penetration-induced) presence of microcracks close to the performed indents, effecting the values obtained from Eq.(1) − (4), resting on half-space theory for homogeneous (crack-free) solid domains. In order to discriminate "damaged" from "non-damaged" halfspaces charcrerized by nanoindentation, the concept of statistical or grid nanoindentation (Constantinides et al., 2006; Constantinides and Ulm, 2007; Ulm et al., 2007) was adopted and modified, in the line of (Kariem et al., 2015): The data for the values of $E_s$ were fitted by $n$ Gaussian Cumulative Distribution Functions (CDFs) with weighting factors $f_j$, $\sum_j^n f_j = 1$, out of which only one represented the intact, undamaged material; namely the one with the largest mean value. The latter was considered as the (average) elastic modulus of undamaged (extracellular) bone tissue. All other Gaussian CDFs represented material damaged to varying extents. This fitting process was repeated for several numbers of phases, and it can be written in mathematical detail as follows: Each one of the $n$ Gaussian CDFs are written in standard form as

$$D_j^{model}(E_s; \mu_j, \sigma_j) = \frac{1}{\sigma_j\sqrt{2\pi}}\int_{-\infty}^{E_s} exp\left(\frac{-(u-\mu_j)^2}{2\sigma_j^2}\right)du \qquad (5)$$

The weighted sum of these distributions is then

$$D^{model}(E_s) = \sum_j^n f_j D_j^{model}(E_s; \mu_j, \sigma_j) \qquad (6)$$

Next, the CDF representing the (sorted) experimental data from nanoindentation, $E_{s,i}$, $i = 1, ..., N$, is constructed according to

$$D^{exp}(E_{s,i}) = \frac{i}{N} - \frac{1}{2N} \qquad (7)$$

with $i \in [1, N]$, $N = 576$ indentations. Optimal fit of the experimental CDF through the superposition of n Gaussian CDFs with mean values mu and standard deviations sigma was obtained through the following minimization problem

$$\mathcal{E} = \sum_{i=1}^N \left(D^{model}(E_{s,i}) - D^{exp}(E_{s,i})\right)^2 \rightarrow min. \qquad (8)$$

The minimization procedure (8) was realized by means of a evolutionary algorithm that starts with a set of approximated CDF parameters (mean $\mu_j$, standard deviation $\sigma_j$ and the weighting factor $f_j$), and, through several so-called "mutation cycles", converges towards the optimal parameters $\mu_j$ and $\sigma_j$, which, for a chosen number $N$ of phases, provide the minimum given in Eq.(8). The algorithm was stopped based on a criterion involving the coefficient of determination, reading as:

$$R^2 = 1 - \frac{\sum_{i=1}^N \left[D^{model}(E_{s,i}) - D^{exp}(E_{s,i})\right]^2}{\sum_{i=1}^N \left[D^{exp}(E_{s,i}) - \frac{1}{N}\sum_{j=1}^N D^{exp}(E_{s,j})\right]^2} \qquad (9)$$

The chosen criterion was inspired by the deliberations of Weicker et al. (2007), and reads as:

$$0.00009 > abs\left[R_k^2 - \left(\frac{1}{1000}\sum_{k-1000}^i R_k^2\right)\right] \qquad \text{AND} \qquad R^2 > 0.98 \qquad (10)$$

with $k$ as the number of mutation cycles; i.e. the attained coefficient of determination is larger than 0.98 and not more 0.00009 different form those attained in the last 1000 mutations.

In order to finally select the optimal number of Gaussian CDFs, $n = o$, for each superposition of Gaussian cumulative distribution functions, the relative error between experimental and model CDF was determined according to

$$e_{rel} = 100 \times \frac{1}{max(E_{s,i}) - min(E_{s,i})} \int_{min(E_{s,i})}^{max(E_{s,i})} \left( D^{model}(E_{s,i}) - D^{exp}(E_{s,i}) \right) dE \quad (11)$$

with $max(E_{s,i})$ and $min(E_{s,i})$ as the maximum and minimum values of the Young modulus obtained from nanoindentation tests, their difference representing the total range of experimental values, while the integral on the right hand side of the equation represents the difference between the $E_{s,i}$ specific values of the model CDF (based on $n$ Gaussians) and of the experimental CDFs. The number of Gaussian distributions $o$ that best fit the experimental data was chosen to be that which resulted in the minimum relative error $e_{rel}$. The corresponding mean value $\mu_0$ is regarded as the undamaged bone tissue modulus, $E_{BT}$.

## 3 Results

### 3.1 Microscopic investigation of the sample surfaces

The initial, coarse polishing of the specimens mainly aimed at milling off enough material, so as to remove a potential tilt of the sample; this left scratch-type traces on the surface, as seen in the light microscopic image of Figure 1, illustrating the only roughly polished, somewhat "scratched" surface of Sample 1. In contrast, subsequent polishing with the 1 μm diamond suspension clearly revealed, under light microscopic magnifications, the finer bone microstructures, see Table 2 for a comparison of different polishing times and resulting surfaces for each of the four samples. The images show no optical differences between the samples finished with different polishing times. All bone samples exhibited a transitional state between plexiform (lamellar) and haversian (osteonal) bone structures, as they are common for young growing cows: stacks of long, parallel lamellae separated by vascular spaces, with osteons in between. (Katz et al., 1984; Locke, 2004).
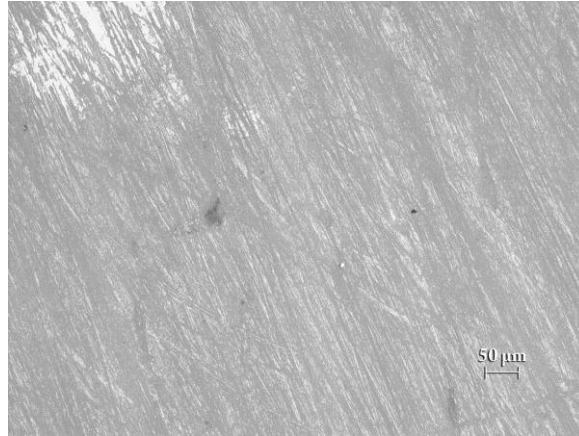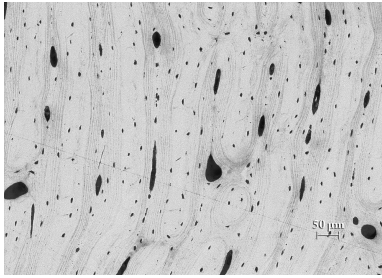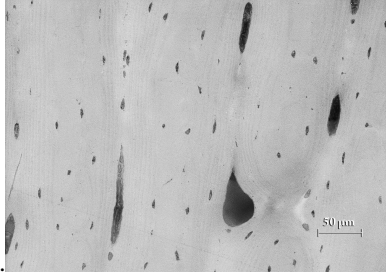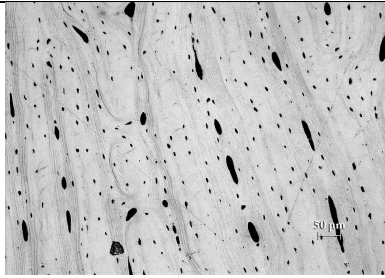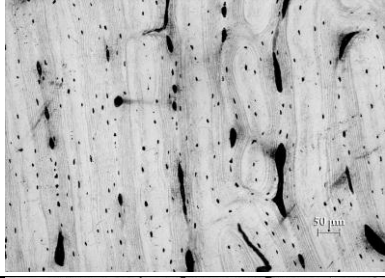
15
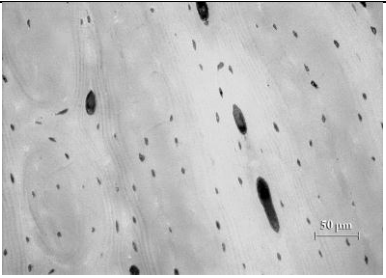
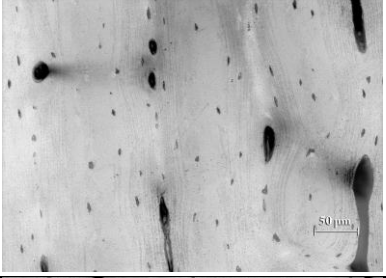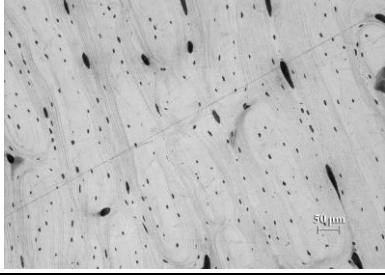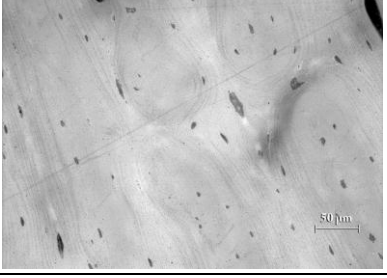Figure 1: The surface of Sample 1 after 3 minute of coarse polishing (particle size 18.3 µm)(100x)

## 3.2 Surface roughness

The roughness determination for the Samples 1 and 4 delivered an average RMS roughness of 11,61 and 9.12 nm, respectively. The results show that the different polishing times (120 and 300 min, respectively) did not result in any significant difference in the average RMS roughness of the samples, the small difference in the two values being due to the variability of the data. With the current protocol, the maximum indentation depth (250 nm) was more than one order of magnitude larger than the average roughness, thus ensuring that the latter does not influence the results of the nanoindentation tests (Bobji and Biswas, 1998). The surface topography of Sample 1 with visible indentation marks is shown in Figure 2.

Table 2: Visual comparison of the four sample surfaces by light microscopy after polishing with 1 µm diamond suspension on a cloth

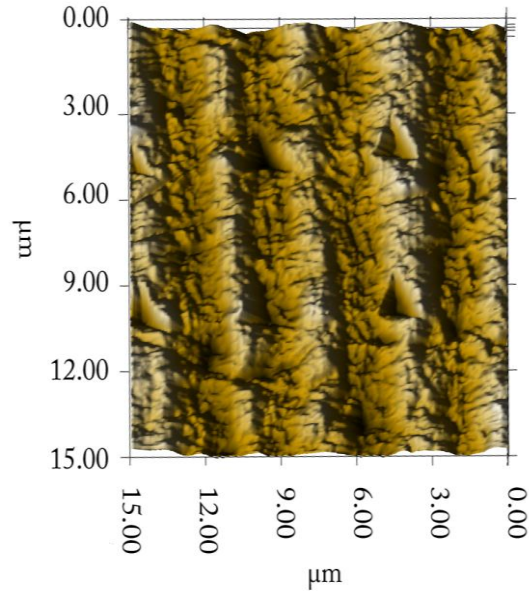| Sample | Polishing time [min] | Surface appearance | |
|---|---|---|---|
| | | 100x magnification | 200x magnification |
| 1 | 120 |  |  |
| 2 | 180 |  |  |
| 3 | 240 |  |  |
| 4 | 300 |  |  |

Figure 2: A surface topography of the indented area of Sample 1 generated in the SPM mode for roughness determination, with visible indentation marks

### 3.3 Undamaged elastic modulus of bovine bone

A. Figure 3 shows all the 576 values for the elastic modulus according to Eq.(4) in ascending order. A typical load-displacement curve for undamaged bone material is shown in Figure 4.
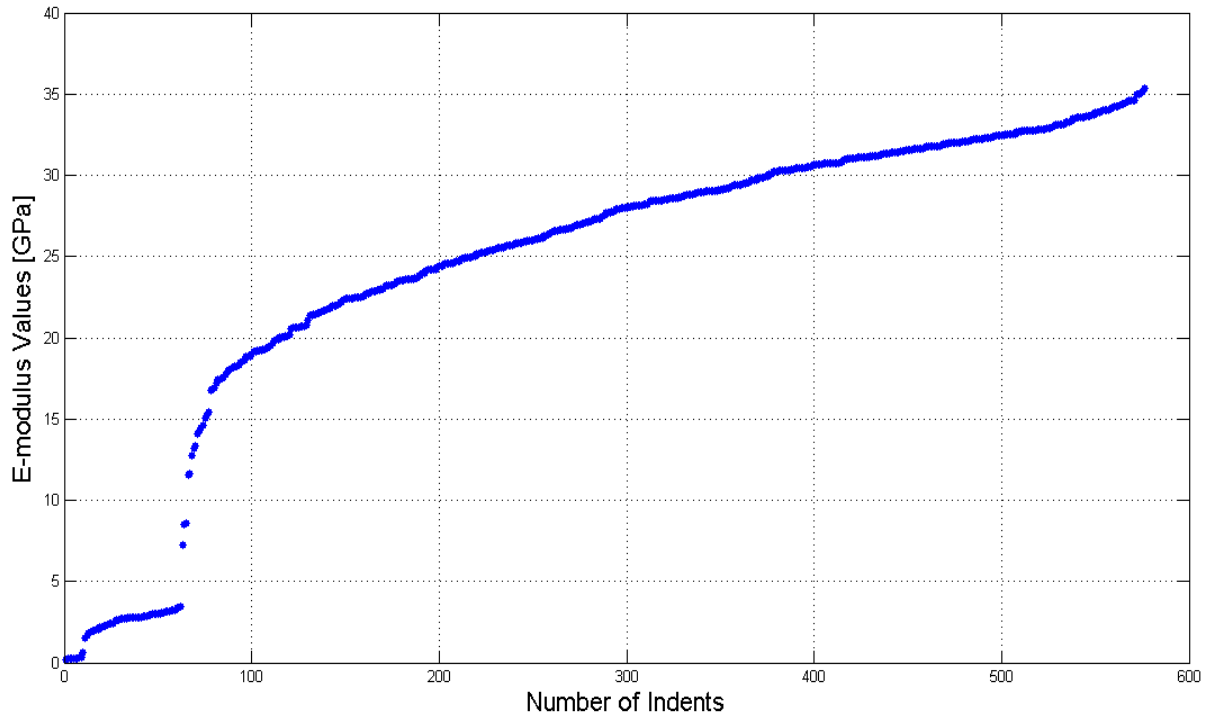


Figure 3: The experimental elastic moduli received from the nanoindentation measurements of cortical bovine femur bone, in ascending order
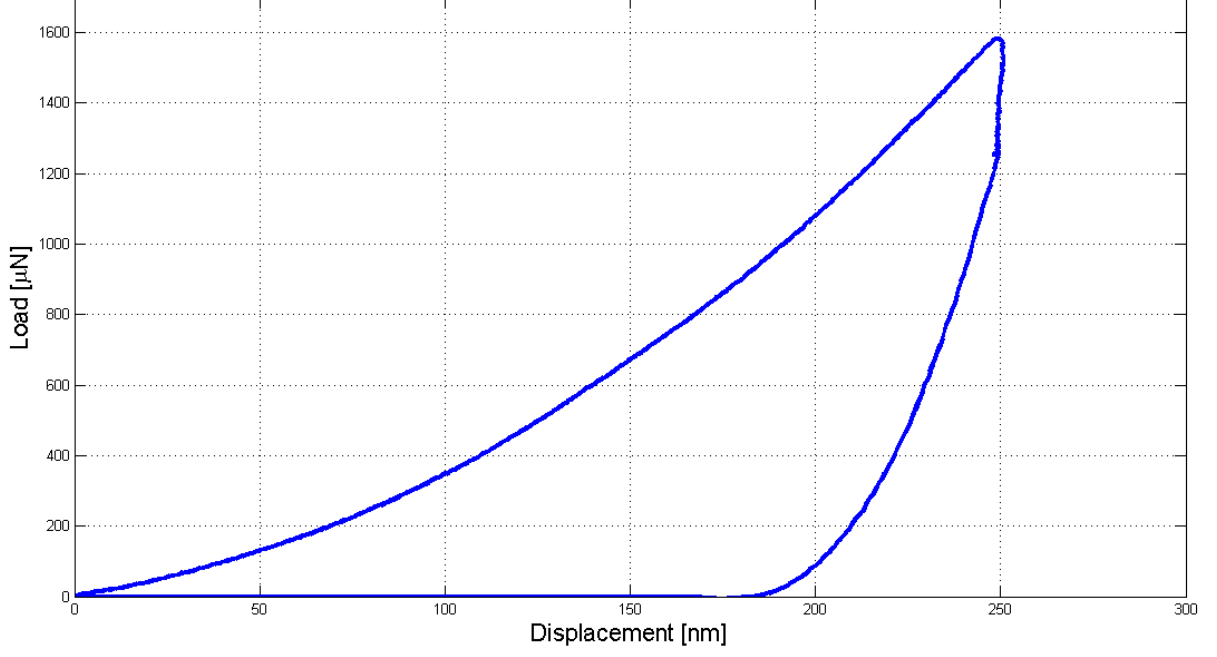
Figure 4: Typical load-displacement curve of a non-damaged cortical bovine femur bone, with an obtained elastic modulus of $E_s$ = 30.53 GPa at 250 nm maximal displacement

With the optimization procedure described in Section 2, all the obtained data was fitted with a number of distributions varying from 1 to 10. The best fit, that minimized the relative error $e_{rel}$ between the experimental and the summed model CDF to 0.62% (see Table 3), was obtained for five distributions, of which four are considered to represent damaged material phases and one corresponds to the intact material; the mean value of the elastic modulus of the latter being the highest of all and thus representing the Young modulus of the undamaged, intact bovine bone material, amounting to $E_{BT}$ = 31.4$\pm$2.5 GPa. The experimental, as well as model single and summed distributions of elastic moduli values are shown as cumulative distribution functions (CDFs) and histograms in Figures 5 and 6, respectively.

Table 3: Results for different numbers of distributions used to fit the experimental data: mean value of the Young modulus for the distribution corresponding to intact bone material ($E_{BT}$); standard deviation ($\sigma$); coefficient of determination ($R^2$); relative error ($e_{rel}$)

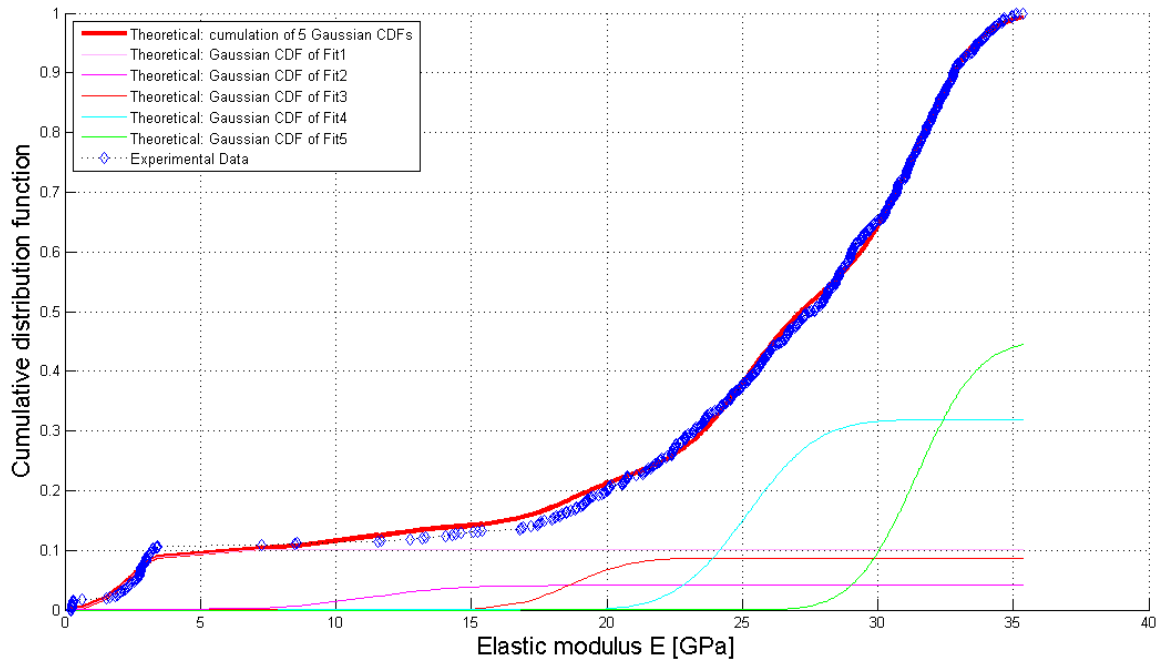| Number of distributions | $E_{BT}$ [GPa] | $\sigma$ | $R^2$ | $e_{rel}$ [%] |
|---|---|---|---|---|
| 1 | 24.6651 | 9.1864 | 0.8891 | 13.7157 |
| 2 | 28.0215 | 5.7494 | 0.9833 | 3.8431 |
| 3 | 29.7854 | 3.0053 | 0.9935 | 2.0848 |
| 4 | 30.8070 | 2.4301 | 0.9957 | 1.1774 |
| **5** | **31.3892** | **2.4858** | **0.9967** | **0.6221** |
| 6 | 31.9549 | 2.0082 | 0.9949 | 0.6587 |
| 7 | 32.2018 | 1.9942 | 0.9943 | 0.6326 |
| 8 | 32.4607 | 1.9967 | 0.9932 | 0.6786 |
| 9 | 32.7463 | 1.9947 | 0.9928 | 0.7211 |
| 10 | 33.8508 | 0.9211 | 0.9899 | 3.3354 |



Figure 5: The Gaussian cumulative distribution functions (CDF) of all experimental data, as well as of the model single and summed distributions
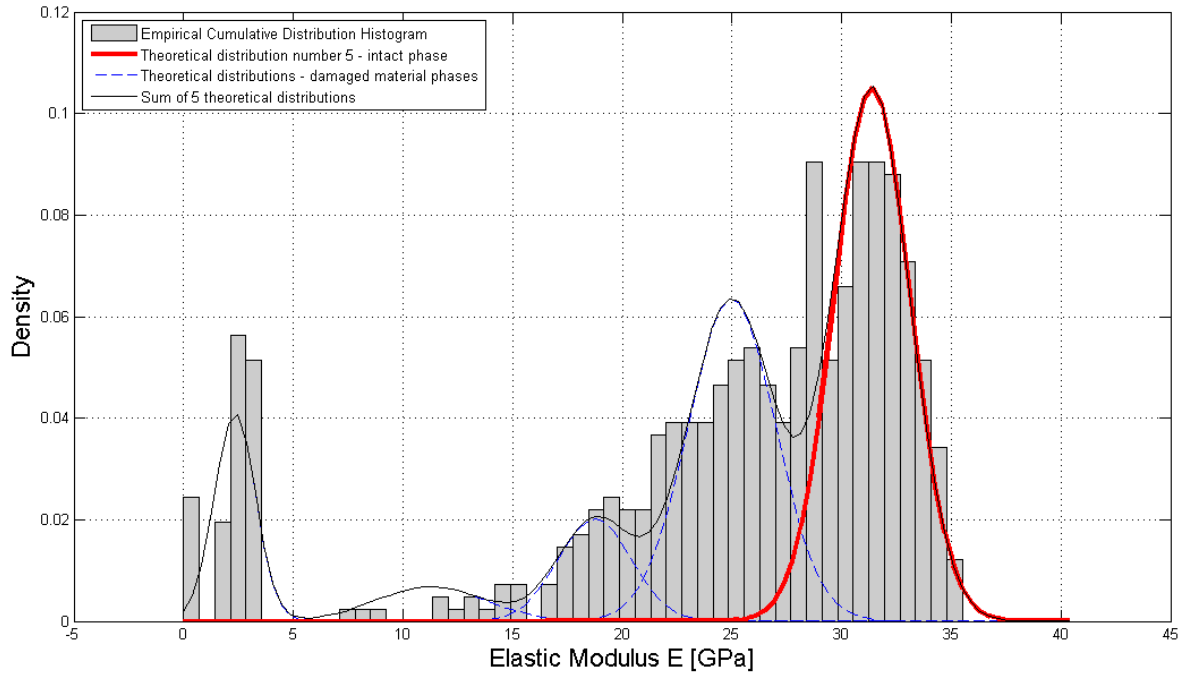
Figure 6: Histogram of experimental values of elastic moduli obtained by nanoindentation and fitting of the data with five distributions, four of them representing damaged material and the last one representing intact bovine bone

## 4    Discussion

We here presented a new method for identification of the undamaged elastic modulus of a solid phase within a (partially) microcracked medium tested through nanoindentation. Therefore, very many indents were performed on bovine bone samples, and the corresponding histogram of elastic moduli was represented in terms of the weighted sum of Gaussian distribution functions.

This representation turned out as very precise, so that the different Gaussians could be interpreted as reflecting the elastic behavior of differently stiff material phases: the stiffest of which would be the undamaged matrix phase, and the others would refer to different levels of mechanical damage. It is interesting to compare our result for the undamaged phase, $E_{BT}$=31.4 ± 2.5 GPa, to independent, alternative experimental results concerning extracellular bovine bone matrix.

In fact, on the very same type of bone, unloading quasi-static tests on SEM-FIB-produced micropillars with only one micron side length and a couple of micrometers height, performed by Luczynski et al (2015), revealed a strikingly similar value, amounting to 29.9 ± 2 GPa.

Furthermore, our results can be compared to the predictions of advanced micromechanical material modeling of bone (Morin and Hellmich, 2014): Feeding the composition and hierarchical interaction rules documented in the aforementioned paper with the bone tissue mass density reported as 2.044 ± 0.43 g/cc (Lees et al., 1979b), yields an axial Young's modulus of bone tissue amounting to 30.1 GPa, again in virtually perfect agreement with the outcome of our new experimental method. Coincidently, this micromechanics model predicts the corresponding axial Poisson's ratio as 0.30; fully confirming the choice of Rietbergen et al. (1995), as used in Section 2.

Finally, the underlying idea of microcracks, either positioned at different distances from the indents (and therefore affecting the result stemming from Oliver and Pharr's half-space problem), or directly emanating from the indents indicated direct sample damaging by the very indentation process, can be checked through observation of indentation processes in an SEM.

A preliminary small number of tests done exactly under these conditions reveal indeed the existence of the aforementioned types of cracks, see Figure 7.
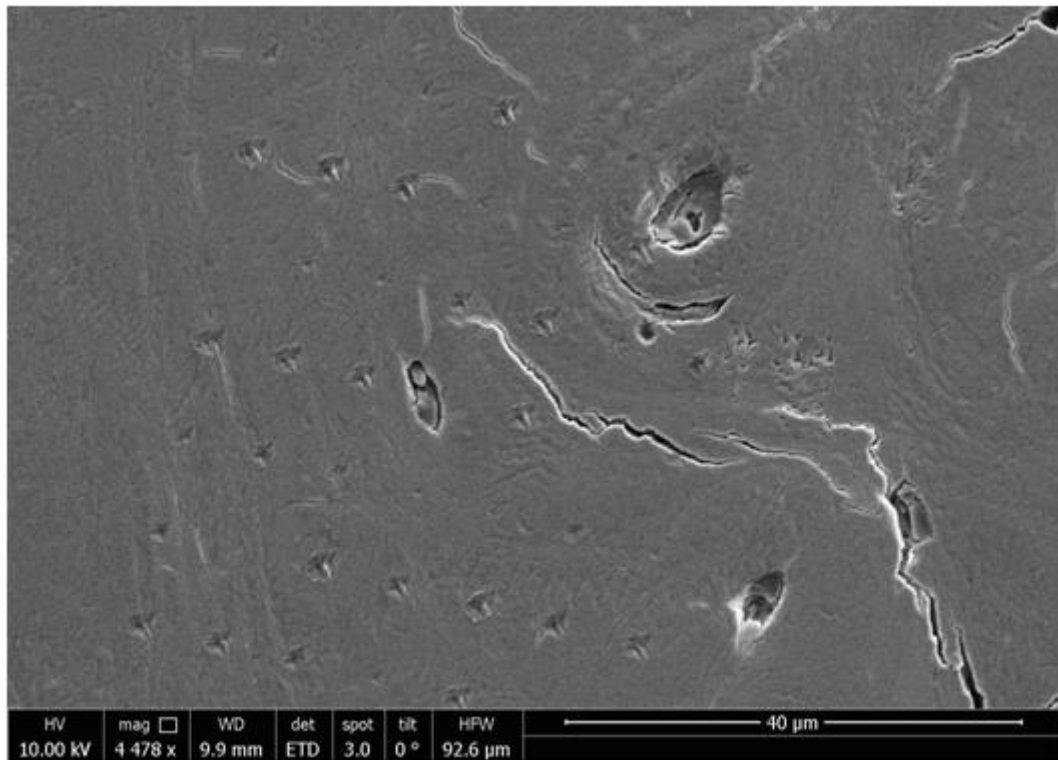


Figure 7: Image made by a Scanning Electron Microscope (SEM) during nanoindentation tests, showing cracks and holes inside the grid of indents

## Acknowledgments

## References

Ashman, R. B., Cowin, S. C., Van Buskirk, W. C., & Rice, J. C., 1984. A continuous wave technique for the measurement of the elastic properties of cortical bone. J. Biomech. 17, 349-361.

Behari, J., 2009. Biophysical Bone Behaviour: Principles and Applications. Singapore: John Wiley & Sons (Asia) Pte Ltd.

Chapurlat, R.D., Arlot, M., Burt-Pichat, B., Chavassieux, P., Roux, J.P., Portero-Muzy, N., Delmas, P.D., 2007. Microcrack Frequency and Bone Remodeling in Postmenopausal Osteoporotic Women on Long-Term Bisphosphonates: A Bone Biopsy Study. J. Bone Miner. Res. 22 (10), 1502–1509.

Constantinides, G., Ravi Chandran, K.S., Ulm, F.-J., Van Vliet, K.J., 2006. Grid indentation analysis of composite microstructure and mechanics: principles and validation. Mater. Sci. Eng. A-Struct. 430, 189–202.

Drugan, W. J., Willis, J. R., 1996. A micromechanics-based nonlocal constitutive equation and estimates of representative volume element size for elastic composites. J. Mech. Phys. Solids 44 (4), 497–524.

Fan, Z., Swadener, J., Rho, J., Roy, M., Pharr, G., 2002. Anisotropic properties of human tibial cortical bone as measured by nanoindentation. J. Orth.Res. 20, 806-810.

Fedorov, F.I., 1968. Theory of Elastic Waves in Crystals. Springer Science + Business Media New York.

Feng, L., Jasiuk, I., 2010. Multi-scale characterization of swine femoral cortical bone. J. Biomech.44 (2), 313–320

Fölsch, C., Mittelmeier, W., Bilderbeek, U., Timmesfeld, N., Von Garrel, T., Matter, H.P., 2011. Effect of Storage Temperature on Allograft Bone. Transfus. Med. Hemother. 39 (1), 36–40."

Fritsch, A., Hellmich, C., 2007. 'Universal' microstructural patterns in cortical and trabecular, extracellular and extravascular bone materials: Micromechanics-based prediction of anisotropic elasticity. J. Theor. Biol. 244 (4), 21, 597–620.

Fritsch, A., Hellmich, C., Dormieux, L., 2009. Ductile sliding between mineral crystals followed by rupture of collagen crosslinks: Experimentally supported micromechanical explanation of bone strength. J. Theor. Biol. 260 (2), 230–252.

Garner, E., Lakes, R., Lee, T., Swan, C.C., Brand, R., 2000. Viscoelastic dissipation in compact bone: implications for stress-induced fluid flow in bone. J Biomech Eng. 122 (2), 166-72.

Hoffler, C.E., Guo, X.E., Zysset, P.K., Goldstein, S.A., 2005. An application of nanoindentation technique to measure bone tissue lamellae properties. J Biomech Eng. 127 (7), 1046-1053.

Hellmich, C., Barthe´le ´my, J.-F., Dormieux, L., 2004. Mineral–collagen interactions in elasticity of bone ultrastructure–a continuum micromechanics approach. European Journal of Mechanics-A/Solids, 23, 783–810.

Hengsberger, S., Kulik, A., Zysset, P., 2002. Nanoindentation discriminates the elastic properties of individual human bone lamellae under dry and physiological conditions. Bone 30 (1), 178–184.

Hengsberger, S., Enstroem, J., Peyrin f., Zysset, P.K., 2003. How is the indentation modulus of bone tissue related to its macroscopic elastic response? A validation study. J. Biomech. 36, 1503–1509.

Hoffler, C.E, Moore, K.E., Kozloff, K., Zysset, P.K., Goldstein, S.A., 2000. Age, gender, and bone lamellae elastic moduli. J. Orthop. Res. 18 (3), 432–437.

Huiskes, R., Weinans, H., Van Rietbergen, B., 1992. The relationship between stress shielding and bone resorption around total hipstems and the effects of flexible materials. Clin. Orthop. Relat. Res. 274, 124–134.

Kariem, H., Pastrama M.-I., Roohani-Esfahani, S.I., Pivonka, P., Zreiqat, H., Hellmich C., 2015. Micro-poro-elasticity of baghdadite-based bone tissue engineering. Mat. Sci. Eng., 553-564.

Katz, L.J., Yoon, H.S, Lipson, S., Maharidge, R., Meunier, A., Christel, P., 1984. The effects of remodeling on the elastic properties of bone. Calcified Tissue International, 36, 31–36.

Kohlhauser, C., Hellmich, C., 2013. Ultrasonic contact pulse transmission for elastic wave velocity and stiffness determination: Influence of specimen geometry and porosity. Eng. Struct. 47, 115–133.

Lees, S., Ahern, J., Leonard, M., 1983. Parameters influencing the sonic velocity in compact calcified tissues of various species. J. Acoust. Soc. Am. 74, 28.

Lees, S., Heeley, J.D., Cleary, P.F., 1979. A study of some properties of a sample of bovine cortical bone using ultrasound. Calcified Tissue International 29 (1), 107-117.

Linde, F., Sørensen, H.C.F., 1993. The effect of different storage methods on the mechanical properties of trabecular bone. J Biomech. 26 (10), 1249-52.

Locke, M., 2004. Structure of Long Bones in Mammals. J. Morphology 262, 546–565.

Lucchini, R., Carnelli, D., Ponzoni, M., Bertarelli, E., Gastaldi, D., Vena, P., 2011. Role of damage mechanics in nanoindentation of lamellar bone at multiple sizes: Experiments and numerical modeling. J. Mech. Beh. Biomed. Mat. 4 (8), 1852-63.

Luczynski, K.W., Steiger-Thirsfeld, A., Bernardi, J., Eberhardsteiner, J., Hellmich, C., 2015. Extracellular bone matrix exhibits hardening elastoplasticity and more than double cortical strength: Evidence from homogeneous compression of non-tapered single micron-sized pillars welded to a rigid substrate. J. Mech. Beh. Biomed. Mat., In Press, Corrected Proof.

Malandrino, A., Fritsch, A., Lahayne, O., Kropik, K., Redl, H., Noailly, J., 2012. Anisotropic tissue elasticity in human lumbar vertebra, by means of a coupled ultrasound-micromechanics approach. Materials Letters 78, 154–158.

Miller, M., Bobko, C., Vandamme, M., Ulm F.-J. 2008. Surface roughness criteria for cement paste nanoindentation. Cement and Concrete Research 38, 467-476.

Morin, C.,Hellmich, C., 2014. A multiscale poromicromechanical approach to wave propagation and attenuation in bone. Ultrasonics, 54, 1251–1269.

Musuvathi, S., Bobji, M.S., Biswas, S.K., 1998. Estimation of Hardness Nanoindentation of Rough Surfaces. J. Mat. Res. 13(11), 3227-3233.

Nazarian, A., Hermannsson, B.J., Muller, J., Zurakowski, D., Snyder, B.D., 2009. Effects of tissue preservation on murine bone mechanical properties. J Biomech. 42 (1), 82-86.

O'Brien, F.J., Taylor, D., Dickson, G.R., Lee, T.C., 2000. Visualisation of three-dimensional microcracks in compact bone. Journal of Anatomy, 197 (03), 413-420.

Oliver, W.C., and Pharr, G.M., 1992. An improved technique for determining hardness and elastic modulus using load and displacement sensing indentation experiments. J.Mater.Res., Vol. 7, 1564-1583.

Ramaniraka, N.A., Rakotomanana, L.R., Leyvraz, P.F., 2000. The fixation of the cemented femoral component: effects of stem stiffness, cement thickness and roughness of the cement – bone surface. J. BoneJointSurg. Br. Vol. 82-B, 297–303.

Reilly, D.T., Burstein, A.H., 1975. The elastic and ultimate properties of compact bone tissue. J. Biomech., 8 (6), Pages 393, Pages IN9, Pages 397-396-IN11-405.

Reisinger, A.G., Pahr, D.H., Zysset, P.K., 2011. Principal stiffness orientation and degree of anisotropy of human osteons based on nanoindentation in three distinct planes. J. Mech. Beh. Biomed. Mat. 4 , 2113-2127.

Rezwan, K., Chen, Q., Blaker, J.J., Boccaccini, A.R., 2006. Biodegradable and bioactive porous polymer / inorganic composite scaffolds for bone tissue engineering. Biomaterials 27, 3413–3431.

Rho, J.Y., Pharr, G.M., 1999. Effects of drying on the mechanical properties of bovine femur measured by nanoindentation. J Mater Sci: Mater Med. 10, 485–488.

Rho, J.Y., Roy, M.E., 1999. Elastic properties of microstructural components of human bone tissue as measured by nanoindentation. J. Biomed. Mat. Res. 45 (1), 48–54.

Rho, J.Y., Zioupos, P., Currey, J.D., Pharr, G.M., 2002. Microstructural elasticity and regional heterogeneity in human femoral bone of various ages examined by nano-indentation. J. Biomech. 35 (2), 189–198.

Rho, J.Y., Tsui, T.Y., Pharr, G.M., 1997. Elastic properties of human cortical and trabecular lamellar bone measured by nanoindentation. Biomaterials 18(20), 1325-1330.

van Rietbergen, B., Weinans, H., Huiskes, R., Odgaard, A., 1995. A new method to determine trabecular bone elastic properties and loading using micromechanical finite-element models. J. Biomech. 28 (1), 69-81.

Ritchie, R., 2011. The conflicts between strength and toughness. Nature Materials 10, 817–822.

Ryan, G., Pandit, A., Apatsidis, D.P., 2006. Fabrication methods of porous metals for use in orthopaedic applications. Biomaterials 27, 2651–2670.

Schaffler, M., Pitchford, W., Choi, K., Riddle, J., 1994. Examination of compact bone microdamage using back-scattered electron microscopy. Bone 15 (5), 483–488.

Schwaiger, C., 2014. Bone elasticity determination: quasi-static unloading tests, ultrasound, and micromechanics. Master's Thesis, Vienna University of Technology (TU Wien).

Schwiedrzik, J., Raghavan, R., Bürki, A., LeNader, V., Wolfram, U., Michler, J., Zysset, P.K., 2014. In situ micropillar compression reveals superior strength and ductility but an absence of damage in lamellar bone. Nature Materials 13, 740–747.

Tai, K., Ulm, F.-J., Ortiz, C., 2006. Nanogranular Origins of the Strength of Bone. Nano Letters, 6 (11), 2520–2525.

Ulm, F.J., Vandamme, M., Bobko, C., Ortega, J.A., Tai, K., Ortiz, C., 2007. Statistical indentation techniques for hydrated nanocomposites: concrete, bone, and shale. J. Am.Ceram. Soc. 90 (9), 2677–2692.

Ulm, F.J., 2007. The nanogranular nature of C–S–H. J. Mech. Phys. Solids 55 (1), 64–90.

Vandamme, M., Ulm, F.J., 2009. Nanogranular origin of concrete creep. PNAS vol. 106 no. 26, 10552-10557.

Vuong, J., Hellmich, C., 2011. Bone fibrillogenesis and mineralization: Quantitative analysis and implications for tissue elasticity. Journal of Theoretical Biology 287, 21, 115–130.

Wang, X.J., Chen, X.B., Hodgson, P.D., Wen, C., 2006. Elastic modulus and hardness of cortical and trabecular bovine bone measured by nanoindentation. Trans. Nonferrous Met. SOC. China 16.

Weicker, K., 2007. Evolutionäre Algorithmen. Leitfäden der Informatik, Vieweg+TeubnerVerlag.

Wenzel, T., Schaffler, M., Fyhrie, D., 1996. In vivo trabecular microcracks in human vertebral bone. Bone 19 (2), 89–95.

Wolfram, U., Wilke, H.J., Zysset, P.K., 2010. Rehydration of vertebral trabecular bone: influences on its anisotropy, its stiffness and the indentation work with a view to age, gender and vertebral level. Bone 46 (2), 348-54.

Yoon, H.S., Katz, J.L., 1976. Ultrasonic wave propagation in human cortical bone-II. Measurements of elastic properties and microhardness. J Biomech. 9 (7), 459-64.

Zaoui, A., 2002. Continuum Micromechanics: Survey. J. Eng. Mech. 128 (8), 808–816.

Zhang, J., Niebur, G.L., Ovaert, T.C., 2008. Mechanical property determination of bone through nano- and micro-indentation testing and finite element simulation. J. Biomech. 41 (2), 267–275.

Zysset, P.K., Edward Guo, X., Edward Hoffler, C., Moore, K.E., Goldstein, S.A., 1999. Elastic modulus and hardness of cortical and trabecular bone lamellae measured by nanoindentation in the human femur. J. Biomech. 32 (10), 1005–1012.

# 3. Additional activities and future work

Roughness measurements and surface scanning of Sample 1 (120 minutes of polishing with a cloth impregnated with 1 μm diamond suspension) and Sample 4 (300 minutes of 1 μm polishing) were made with the TriboIndenter equipment of Hysitron at a scanning rate of 3 Hz. The topographic images were made at different locations using scan sizes of 15 μm× 15 μm2. Table 3 shows a summary of the roughness measurement results. The surface scan was repeated to visually examine the indentations, the topographic image of which can be found in the paper. Figure 1 shows image statistics, as well as surface scanning pictures from the Hysitron software.

Table 3: Results of roughness calculation (Projected Area = scanned area; RMS Roughness = Root Mean Squared Roughness; Peak-to-Valley = Max Height – Min Height)

|  | Sample 1 | Sample 4 |
|---|---|---|
| 1. | Projected Area = 225 μm^2<br>RMS Roughness (Rq) = 6.30226 nm<br>Average Roughness (Ra) = 5.00147 nm<br>Mean Height = -0.0225375 nm<br>Max Height = 18.2878 nm<br>Min Height = -26.6414 nm<br>Peak-to-Valley = 44.9292 nm | Projected Area = 225 μm^2<br>RMS Roughness (Rq) = 9.60791 nm<br>Average Roughness (Ra) = 6.75024 nm<br>Mean Height = -0.0126778 nm<br>Max Height = 50.6187 nm<br>Min Height = -48.8577 nm<br>Peak-to-Valley = 99.4764 nm |
| 2. | Projected Area = 225 μm^2<br>RMS Roughness (Rq) = 16.9212 nm<br>Average Roughness (Ra) = 13.9889 nm<br>Mean Height = 0.00886825 nm<br>Max Height = 43.2585 nm<br>Min Height = -48.6319 nm<br>Peak-to-Valley = 91.8904 nm | Projected Area = 225 μm^2<br>RMS Roughness (Rq) = 8.62437 nm<br>Average Roughness (Ra) = 6.9733 nm<br>Mean Height = -0.0143238 nm<br>Max Height = 25.1513 nm<br>Min Height = -29.4411 nm<br>Peak-to-Valley = 54.5924 nm |
| AVG | Average RMS = 11,61 nm | Average RMS = 9,12 nm |
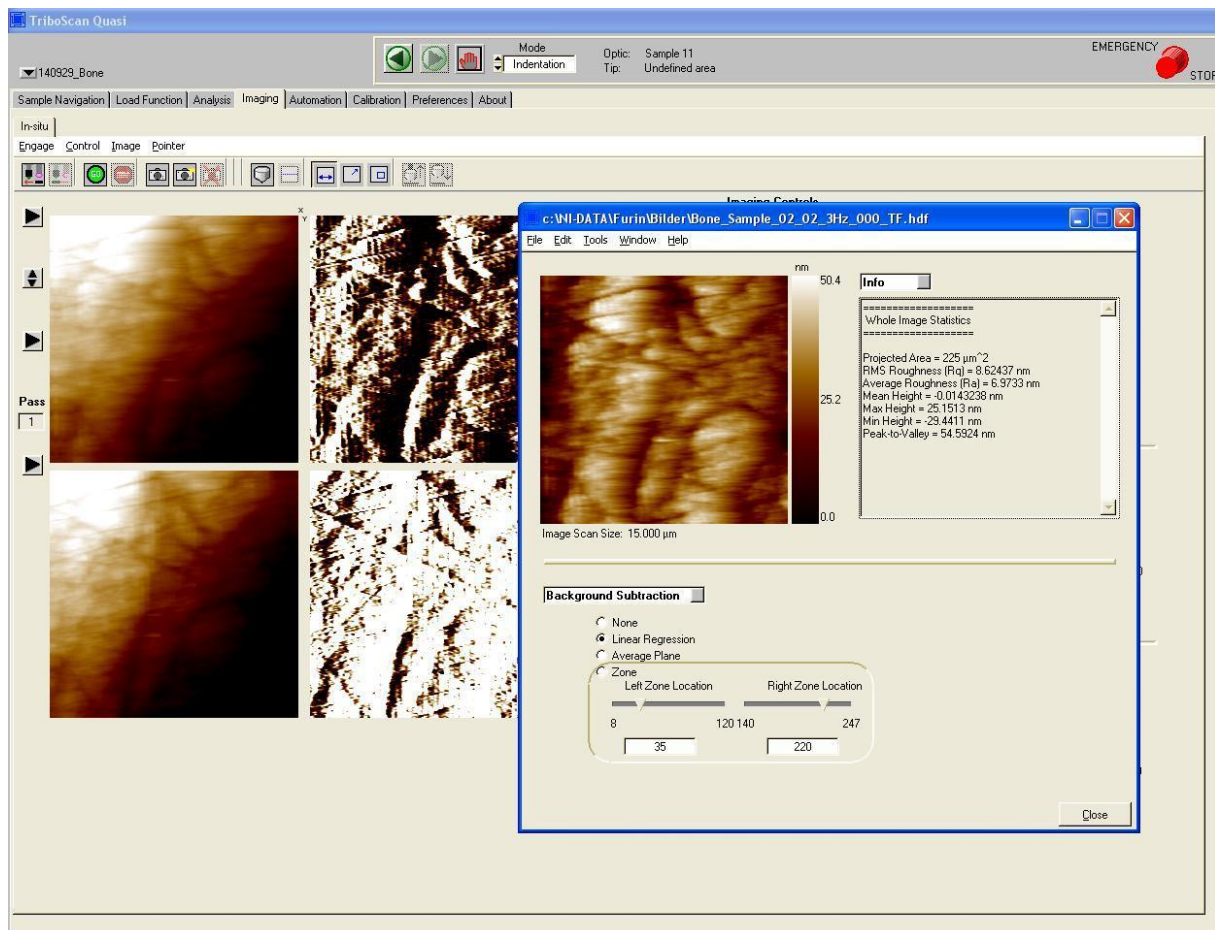
Figure 1: Roughness measurement and surface scanning

For future work it could be of great interest to work out the possibilities of a visual examination of the damages that may occur as a result of sample preparation or during the nanoindentation process. An initiative of picoindentation tests (PI 85 Picoindenter, Hysitron, shown in Figure 2) and high resolution imaging in a Scanning Electron Microscope (SEM) environment at nanometer scale has already been started by the Institute for Mechanics of Materials and Structures, in collaboration with USTEM (Service Center for Transmission and Electronmicroscopy) at the Vienna University of Technology.

Figure 2: Picoindenter mounted on the SEM stage

The following images present the indentation process in vivo. Figure 3 demonstrates as the indentor tip approaches the sample surface, while Figure 4 shows the surface, with the clearly detectable indentation grid. It is hoped that, in the future, the correlation of such images with the results obtained from picoindentation tests could give additional information on the existence of damage in the tested samples (pre- or post-testing). This could shed light on the dynamics of the cracking and damaging processes, and how exactly these affect the determination of elastic material properties from nanoindentation tests.
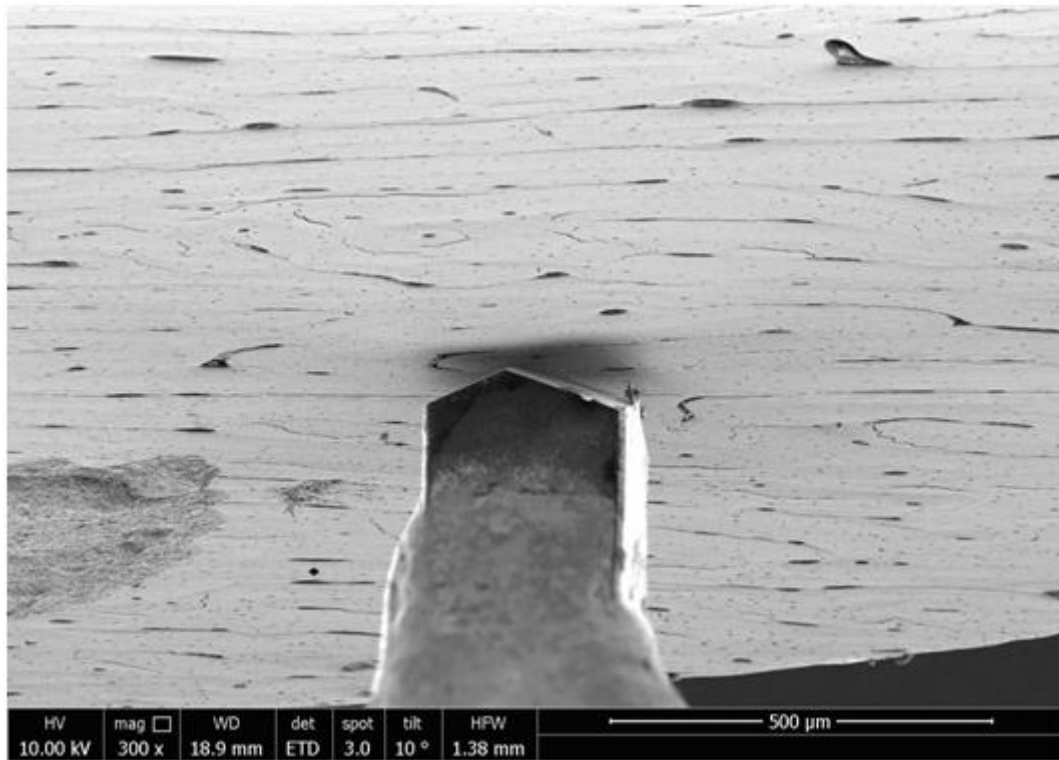
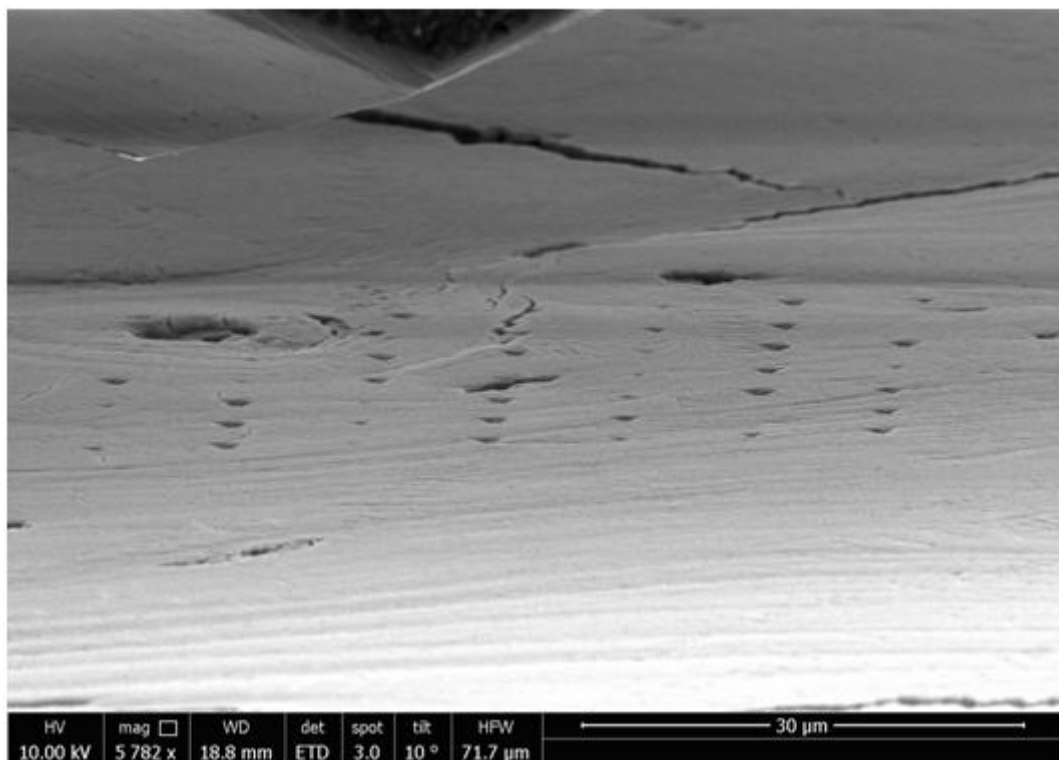Figure 3: Sample indentation inside picoindentor



Figure 4: Sample indentation inside picoindentor with the indentation matrix visible

# A. Appendix I: Microscopic images of the samples

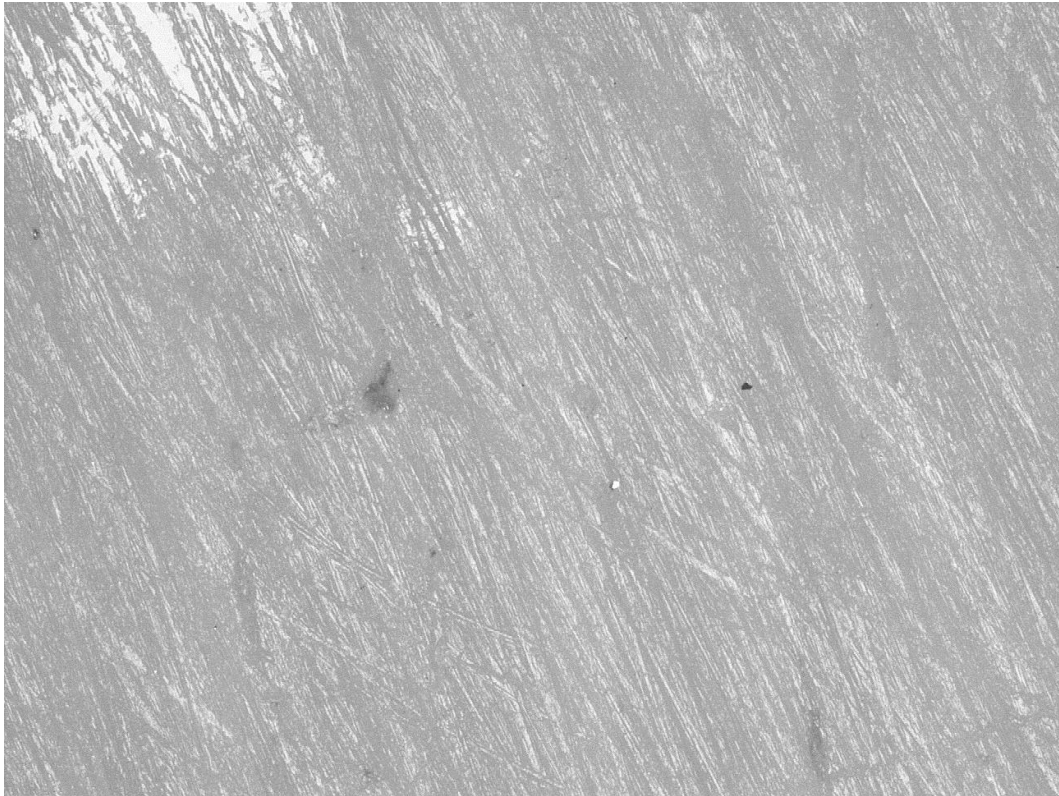High resolution microscope pictures of prepared bovine femur bone samples.



Figure 5: The surface of Sample 1 after 3 minute grinding with 1000 $\mu$m diamond grit



Figure 6: Sample 1 after 120 min of polishing with cloth sprayed with 1 µm diamond suspension (100x magnification)

Figure 7: Sample 1 after 120 min of polishing with cloth sprayed with 1 μm diamond suspension (200x magnification)



Figure 8: Sample 2 after 180 min of polishing with cloth sprayed with 1 μm diamond suspension (100x magnification)

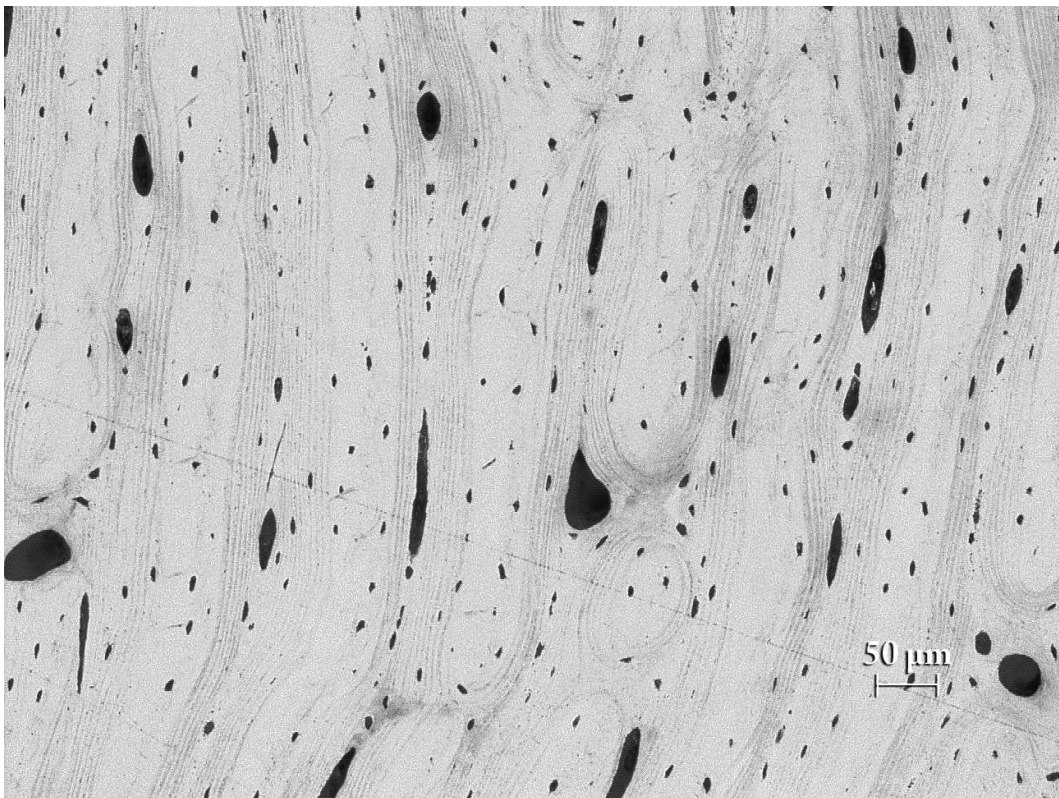Figure 9: Sample 2 after 180 min of polishing with cloth sprayed with 1 µm diamond suspension (200x magnification)



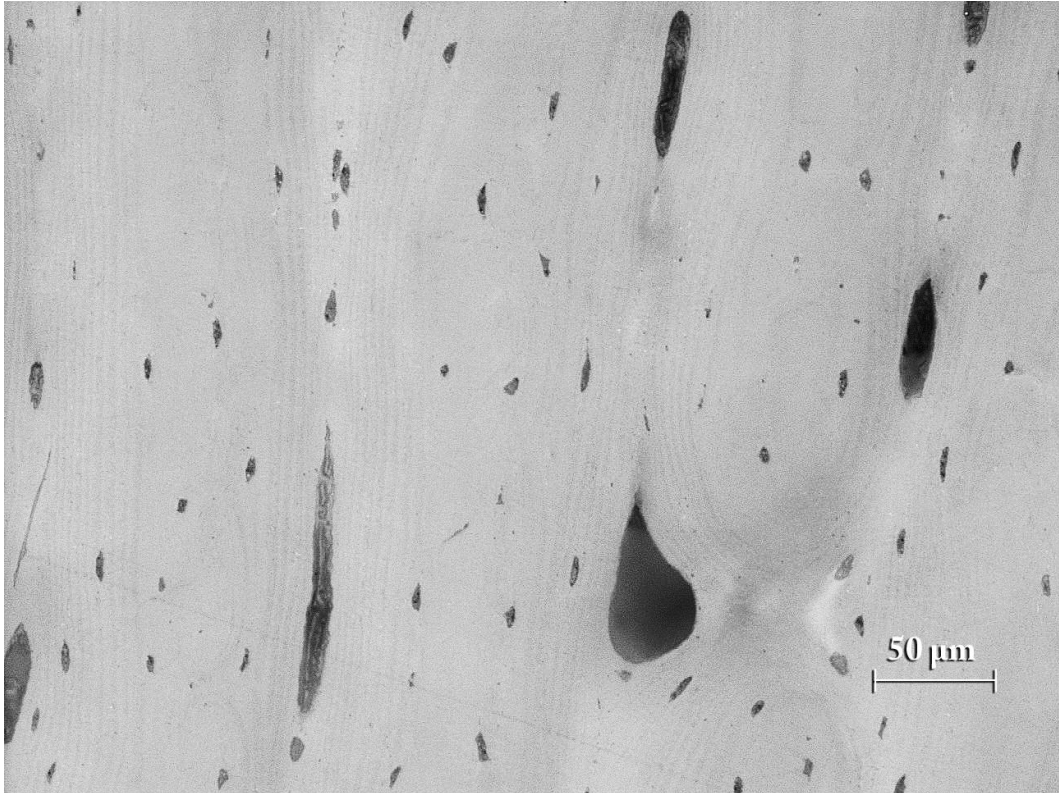Figure 10: Sample 3 after 240 min of polishing with cloth sprayed with 1 µm diamond suspension (100x magnification)

Figure 11: Sample 3 after 240 min of polishing with cloth sprayed with 1 μm diamond suspension (200x magnification)



Figure 12: Sample 4 after 300 min of polishing with cloth sprayed with 1 μm diamond suspension (100x magnification)

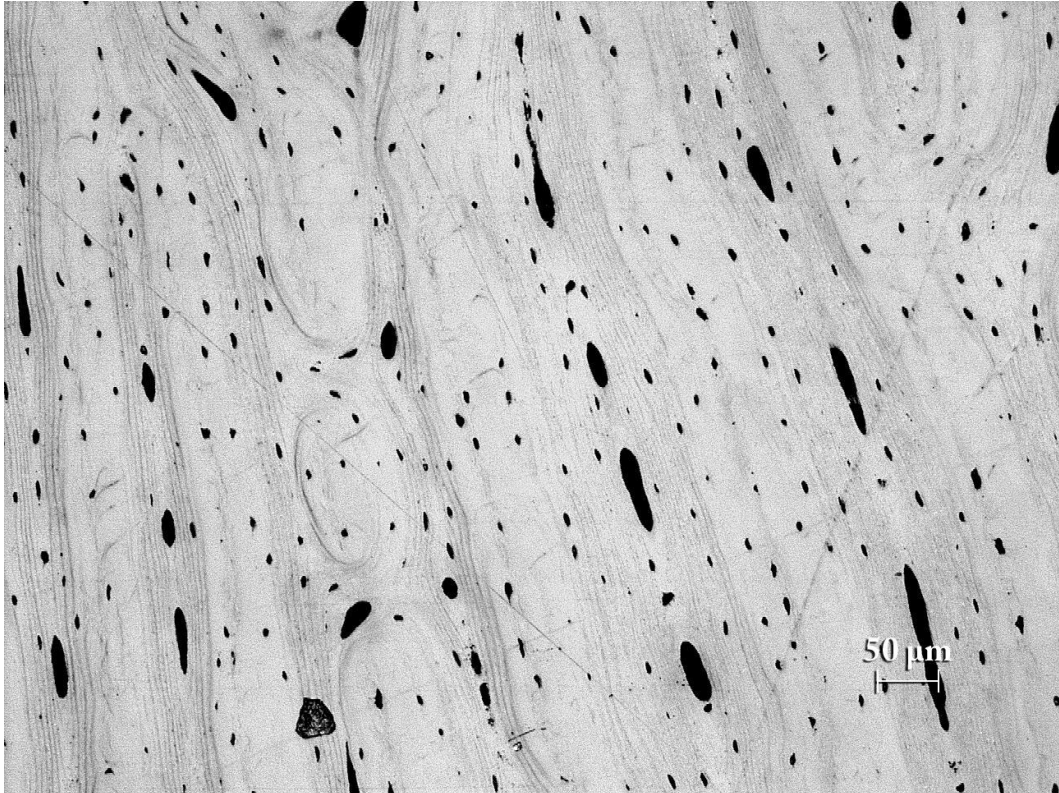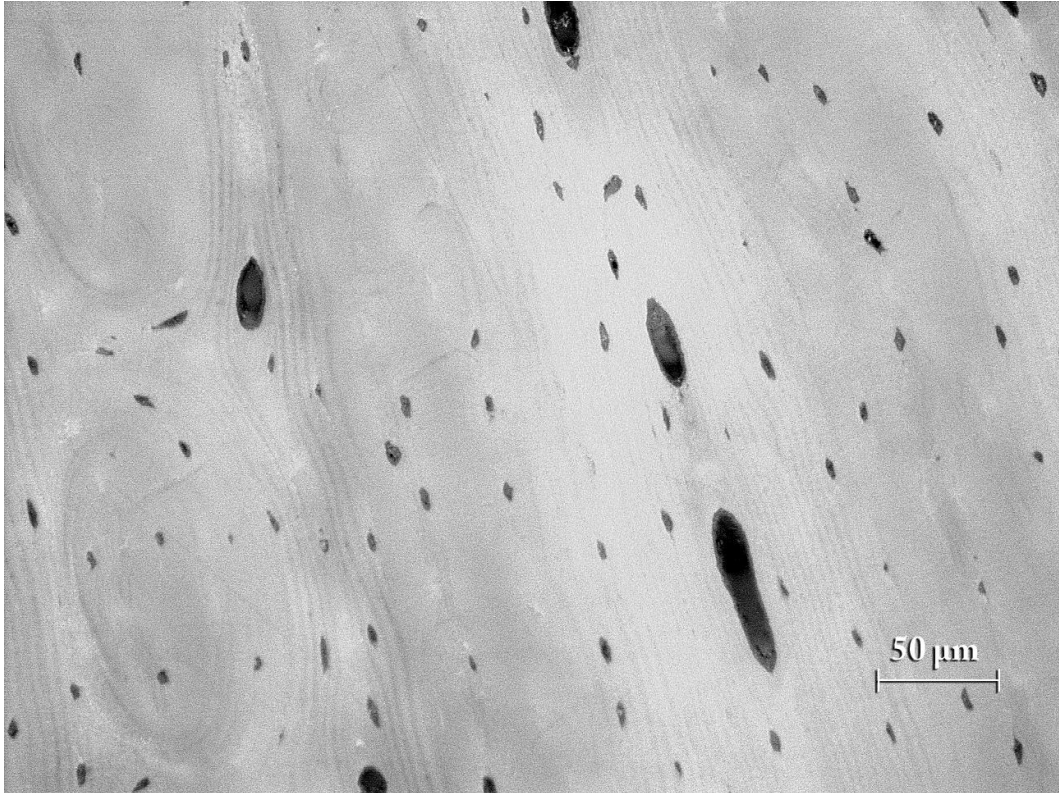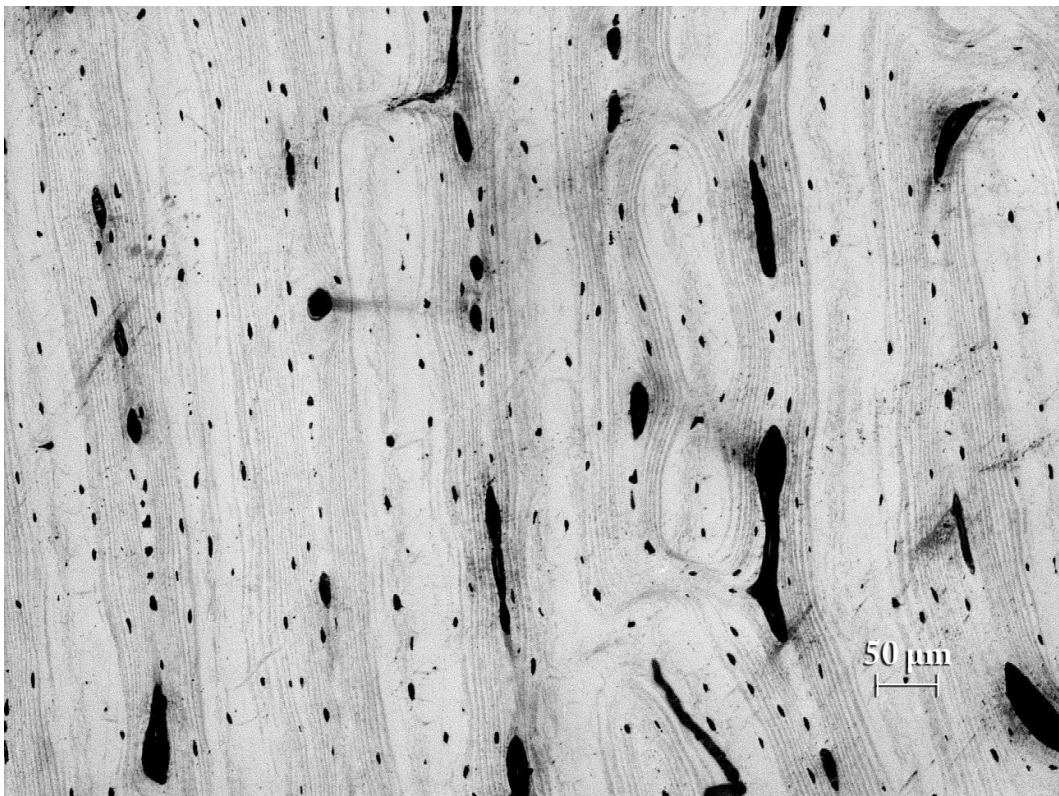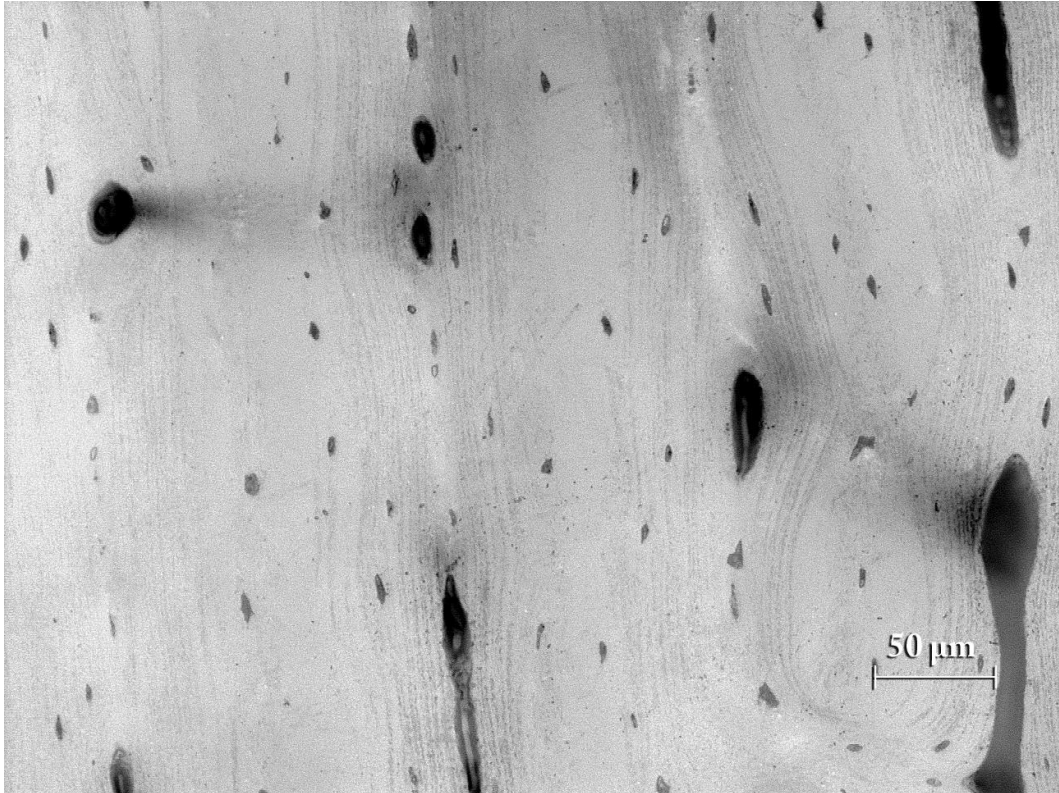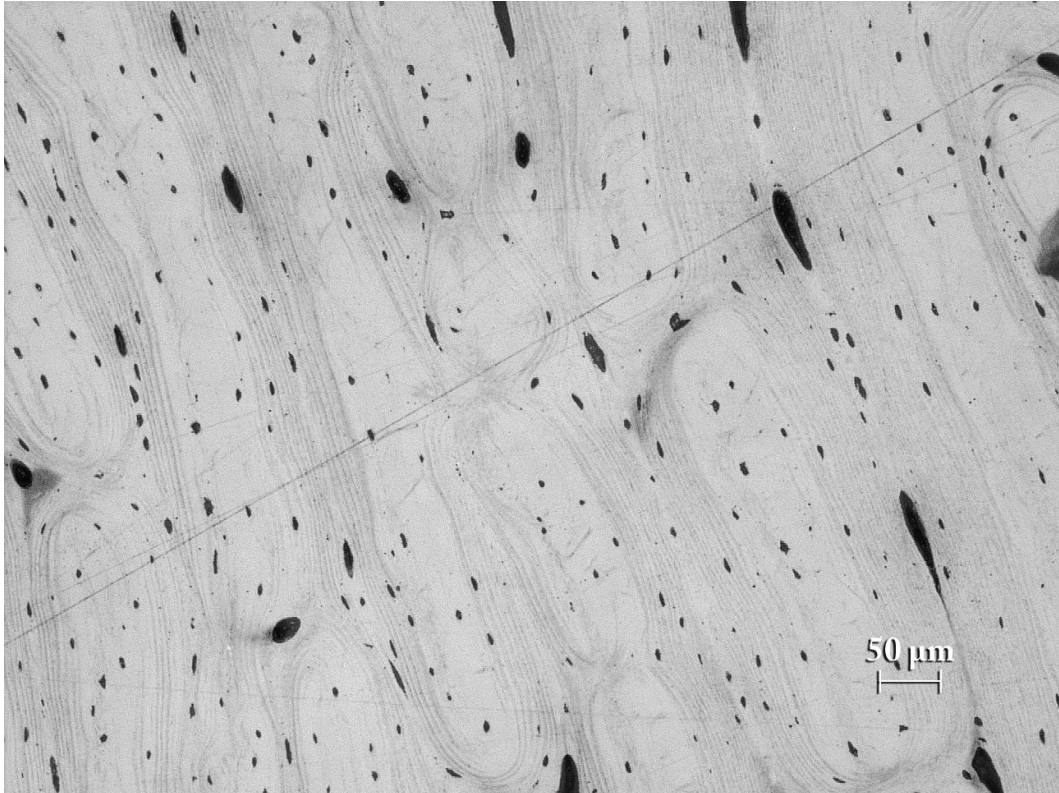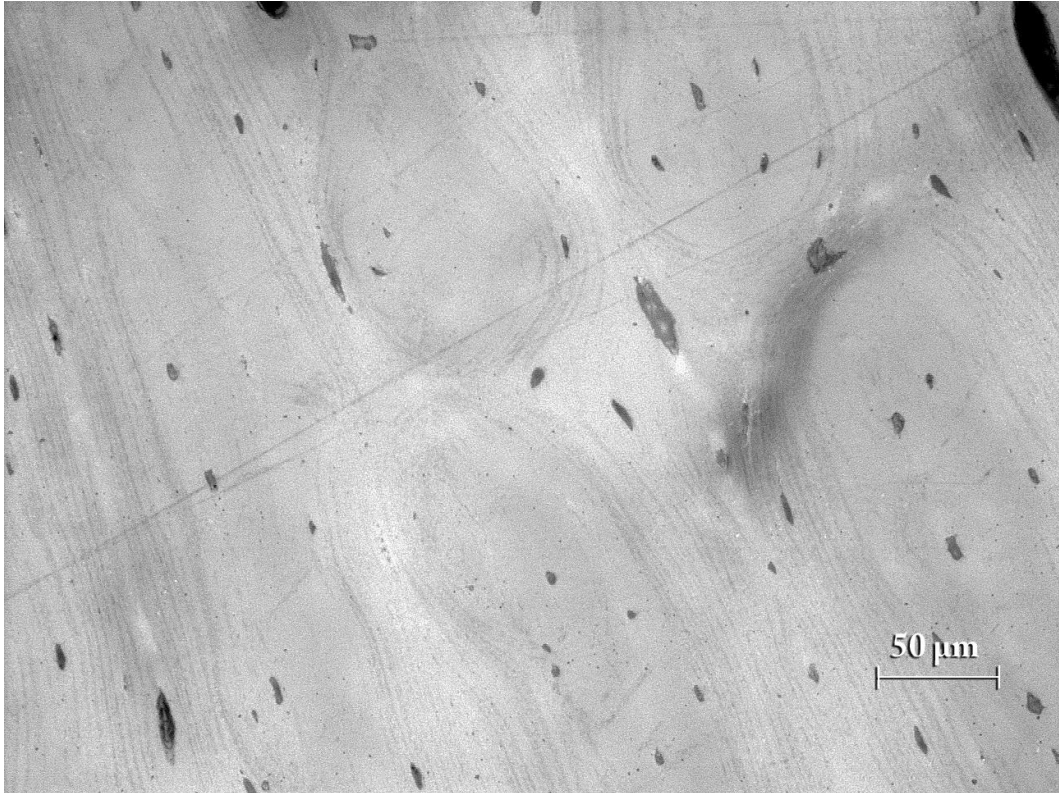Figure 13: Sample 4 after 300 min of polishing with cloth sprayed with 1 µm diamond suspension (200x magnification)

# B. Appendix II: Matlab source code used to identify the Young modulus of the damaged and undamaged material phases

## Script

The main script initiates function "Sample_all" a given number of times, in order to define the convergence value of the means of $E, \sigma, R^s$ and $e_{rel}$.

```matlab
clear all;
my_files={'Sample_all.m'}; %'Sample_1.m''Sample_2.m''Sample_3.m''Sample_4.m'
ntimes=100; %The number of runs
n=ntimes;
str_n=num2str(ntimes);
Max_number_of_fits=10; %The maximum number of distributions, we would like to analyze
    e_ntimes=zeros(Max_number_of_fits,n+1);
    sigma_ntimes=zeros(Max_number_of_fits,n+1);
    r2_ntimes=zeros(Max_number_of_fits,n+1);
    rel_err_ntimes=zeros(Max_number_of_fits,n+1);
    e_ntimes(:,1)=(1:1:Max_number_of_fits)';
    sigma_ntimes(:,1)=(1:1:Max_number_of_fits)';
    r2_ntimes(:,1)=(1:1:Max_number_of_fits)';
    rel_err_ntimes(:,1)=(1:1:Max_number_of_fits)';

for n=1:ntimes
    filename=char(my_files);
    [Results,e]=Sample_all(Max_number_of_fits);
    e_ntimes(:,n+1)=Results(:,2);
    sigma_ntimes(:,n+1)=Results(:,3);
    r2_ntimes(:,n+1)=Results(:,4);
    rel_err_ntimes(:,n+1)=Results(:,5);
end

    mean_e=mean(e_ntimes(:,2:end),2);
    mean_sigma=mean(sigma_ntimes(:,2:end),2);
    mean_r2=mean(r2_ntimes(:,2:end),2);
    mean_rel_err=mean(rel_err_ntimes(:,2:end),2);

    Results_means=[(1:Max_number_of_fits)',mean_e,mean_sigma,mean_r2,mean_rel_err];
```

```matlab
    %plot the E, std, R2 and rel_err means by number of distributions
clf;
f=figure;
hold on;
x=1:Max_number_of_fits;
Y = Results_means(:,4);
grid on
hArray = plot(x,Y,'-rs','LineWidth',2,'MarkerEdgeColor','k','MarkerFaceColor','k','MarkerSize',5);
set(gca,'XLim',[0 Max_number_of_fits+1],'Layer','top')
xlabel('Number of fitted curves','FontSize',14)
ylabel('Coefficient of Determination','FontSize',14)
title(['Mean of Coefficient of Determination for ',str_n,' Mutation Cycles'],'FontSize',16)
print(f,'-dtiff',['All_data_',str_n,'_times_R2.tiff']);


clf;
f=figure;
hold on;
x=1:Max_number_of_fits;
Y = Results_means(:,5);
grid on
hArray = plot(x,Y,'-rs', 'LineWidth',2,'MarkerEdgeColor','k','MarkerFaceColor','k','MarkerSize',5);
set(gca,'XLim',[0 Max_number_of_fits+1],'Layer','top')
xlabel('Number of fitted curves','FontSize',14)
ylabel('Relative Error','FontSize',14)
title(['Mean of Ssq of Relative Error for ',str_n,' Mutation Cycles'],'FontSize',16)
print(f,'-dtiff',['All_data_',str_n,'_times_rel_err.tiff']);


clf;
f=figure;
hold on;
x=1:Max_number_of_fits;
Y = Results_means(:,2);
grid on
hArray = plot(x,Y,'-rs', 'LineWidth',2,'MarkerEdgeColor','k','MarkerFaceColor','k','MarkerSize',5);
set(gca,'XLim',[0 Max_number_of_fits+1],'Layer','top')
xlabel('Number of fitted curves','FontSize',14)
ylabel('E-Modulus [GPa]','FontSize',14)
title(['Mean of E-Modulus for ',str_n,' Mutation Cycles'],'FontSize',16)
print(f,'-dtiff',['All_data_',str_n,'_times_E.tiff']);
```

```matlab
clf;
f=figure;
hold on;
x=1:Max_number_of_fits;
Y = Results_means(:,3);
grid on
hArray = plot(x,Y,'-rs', 'LineWidth',2,'MarkerEdgeColor','k','MarkerFaceColor','k','MarkerSize',5);
set(gca,'XLim',[0 Max_number_of_fits+1],'Layer','top')
xlabel('Number of fitted curves','FontSize',14)
ylabel('Sigma','FontSize',14)
title(['Mean of Sigma (E-Modulus) for ',str_n,' Mutation Cycles'],'FontSize',16)
print(f,'-dtiff',['All_data_',str_n,'_times_sigma.tiff']);
close(f);

%%Plot the way, the means stabilize after a number of runs to adjust the number of necessary runs
%Rel_error means
AA=zeros(Max_number_of_fits,(n-1));
fig=figure;
hold on
x=(1:(n-1));
LegHandles = []; LegText = {};
Fit_color=[1 .7 .5;1 0 1;1 0 0;0 1 1;0 1 0;0 0 1;0 0 0;0.5 0.5 1;0.5 0 0.5;0 0.5 1];
for j=1:Max_number_of_fits
    jstr=num2str(j);
    for i=1:size(rel_err_ntimes,2)-2
        F=sum(rel_err_ntimes(j,2:i+2)/(i+1));
        AA(j,i)=F;
    end
    hLine=plot(x,AA(j,:),'Color',Fit_color(j,:),'LineStyle','-', 'LineWidth',2,'Marker','none', 'MarkerSize',6);
        LegHandles(end+1) = hLine;
        LegText{end+1} = ['Means of relative error',jstr];
end
xlabel('number','FontSize',14)
ylabel('means of relerr','FontSize',14)
hLegend = legend(LegHandles,LegText,'Orientation', 'vertical', 'Location', 'NorthWest');
printname=['means_rel_err_',str_n,'runs.tiff'];
print(fig,'-dtiff',printname)
hold off;

%R2 means
BB=zeros(Max_number_of_fits,(n-1));
```

```matlab
fig=figure;
hold on
x=(1:(n-1));
LegHandles = []; LegText = {};
Fit_color=[1 .7 .5;1 0 1;1 0 0;0 1 1;0 1 0;0 0 1;0 0 0;0.5 0.5 1;0.5 0 0.5;0 0.5 1];
for j=1:Max_number_of_fits
    jstr=num2str(j)
    for i=1:size(r2_ntimes,2)-2
        F=sum(r2_ntimes(j,2:i+2)/(i+1));
        BB(j,i)=F;
    end
    hLine=plot(x,BB(j,:),'Color',Fit_color(j,:),'LineStyle','-', 'LineWidth',2,'Marker','none', 'MarkerSize',6);
        LegHandles(end+1) = hLine;
        LegText{end+1} = ['Means of R^2 Fit',jstr];
end
xlabel('number','FontSize',14)
ylabel('means of R^2','FontSize',14)
hLegend = legend(LegHandles,LegText,'Orientation', 'vertical', 'Location', 'SouthEast');
printname=['means_r2_',str_n,'runs.tiff'];
print(fig,'-dtiff',printname)
hold off;
h=msgbox('We''re ready!');
save(['Sample_all_',str_n,'times.mat']);
```

# Function "Sample_all"

Function "Sample_all" calculates the elastic modulus of the undamaged material phase and provides the coefficient of determination and the relative error of the fitted, weighted normal cumulative distribution functions for a different number of fitting curves.

```
function[Results,e]=Sample_all(Max_number_of_fits)

filename='Sample_all_E_calculated';
load(filename,'emodulus');

e=sort(emodulus);
e=unique(e);
e=e';
fits_data=struct();
a=0.001;  %initial p (mean and std deviation) scatter ratio
b=1;      %initial weight scatter ratio
Results=zeros(Max_number_of_fits,5);
 Fit_color=[1 .7 1;1 0 1;1 0 0;0 1 1;0 1 0;0 0 1;0 0 0;0.5 0.5 1;0.5 0 0.5;0 0.5 1];


% plot original values
  fig=figure;
  grid on;
  plot(e);
  title('Original E-modulus Data from Indentation Experiments');
  xlabel('Number of Indents');
  ylabel('E-modulus Values [GPa]');
  print(fig,'Sample_all_E_modulus.tiff','-dtiff');
  close(fig);

% ECDF - Empirical Cumulative Distribution Function of measured E moduli
[f,x_e]=ecdf(e);
f=f';
x_e=x_e';

mean_f=sum(f)/length(f);
sst=sum((f-mean_f).^2);

% NCDF - Normal Cumulative Distribution Function fitted on the original data
```

```matlab
for fits=1:Max_number_of_fits
    fits_str=['fit',num2str(fits)];
    Printfn=['Sample_all_estimated_pd',fits_str,'.tiff'];

    % CreateFit - We create estimated parent values of mu and sigma of normal distribution fits
    [pd_mean,pd_std]=CreateFit(emodulus,Printfn,fits);
    fits_data.(fits_str).p_mean=pd_mean;
    fits_data.(fits_str).p_std=pd_std;
    fits_data.(fits_str).r2=0;


%Initiating the Mutate function based on the parent values from the CreateFit function
    c=a; %initial scatter ratio for mean and std will be adjusted
    d=b; %initial scatter ratio for weight will be adjusted
    k=1; % break

 while fits_data.(fits_str).r2<0.98
    if fits==1 && fits_data.(fits_str).r2>0.8
     break
    end
   fits_data.(fits_str).w=zeros(1,fits);
   for i=1:fits
     fits_data.(fits_str).w(i)=1/fits;
   end
 % Mutate – evolution of ncdfs
[ncdf_p,ncdf_p_fits,p_mean,p_std,w,ssr,r2]=Mutate(fits_data.(fits_str).p_mean,fits_data.(fits_str).p_std,fits_data.(fits_str).w,e,f,sst,fits,c,d);
fits_data.(fits_str).ncdf=ncdf_p;
fits_data.(fits_str).ncdf_fits=ncdf_p_fits;
fits_data.(fits_str).p_mean=p_mean;
fits_data.(fits_str).p_std=p_std;
fits_data.(fits_str).w=w;
fits_data.(fits_str).ssr=ssr;
fits_data.(fits_str).r2=r2; %coefficient of determination
   c=c*1.2; %scatter ratio for mean and std
   k=k+1;
   if k>100
     d=d*1.2; %scatter ratio for weight
     if k==300
      break
```
42

```matlab
    end
  end
 end


% relative error
E_max=max(e);
E_min=min(e);
Integral_ncdf=trapz(ncdf_p,e);
Integral_ecdf=trapz(f(2:end),e);
fits_data.(fits_str).rel_err=abs(Integral_ncdf-Integral_ecdf)/(E_max-E_min)*100;


% %plot the mutated weighted distributions
Printfn=['Sample_all_fitted_pd_',fits_str,'.tiff'];
[Fit]=PrintFit(emodulus,fits_data.(fits_str).p_mean,fits_data.(fits_str).p_std,w,Printfn,fits);


% %plot the cumulated mutated weighted ncdfs
figure
hold on;
 LegHandles = []; LegText = {};
 str_i=num2str(fits);
 hLine = plot(e,fits_data.(fits_str).ncdf,'LineWidth',3,'Color','Red');
 LegHandles(end+1) = hLine;
 LegText{end+1} = ['Theoretical: cumulation of ',str_i,' Gaussian CDFs'];
hold all
   for i=1:fits
   hLine = plot(e,fits_data.(fits_str).ncdf_fits(:,i)*fits_data.(fits_str).w(i),'LineWidth',1,'Color',Fit_color(i,:));
   LegHandles(end+1) = hLine;
   str_i=num2str(i);
   LegText{end+1} = ['Theoretical: Gaussian CDF of Fit',str_i];
   hold on
   end
 hLine = plot(x_e,f,'MarkerEdgeColor','b','MarkerFaceColor','b','MarkerSize',10);
   LegHandles(end+1) = hLine;
   LegText{end+1} = 'Experimental Data';
hold off
set(gca,'XTick')
   hLegend = legend(LegHandles,LegText,'Orientation', 'vertical', 'Location', 'NorthWest');
   set(gca,'XTickLabel')
   title('ECDF &  NCDF, Empirical and Normal Cumulative Distribution Functions of all Samples');
   xlabel('Elastic modulus E [GPa]');
```

```matlab
    ylabel('Cumulative distribution function');
    grid on;
    Printfn=['Sample_all_ecdf_',fits_str,'_ncdf.tiff'];
    print(figure,'-dtiff',Printfn);
    Printfn=['Sample_all_ecdf_',fits_str,'_ncdf.fig'];
close(figure);

%%Acquiring output data – mean, std, r2 and relative error
Results(fits,:)=[fits,max(fits_data.(fits_str).p_mean),max(fits_data.(fits_str).p_std),fits_data.(fits_str).r2,fits_
data.(fits_str).rel_err];
end
save('Sample_all_experiment.mat');
end
```

# Function "CreateFit"

Function "CreateFit" creates evenly distributed Gaussian probability distribution functions (pdf) on the original data, according to the required number of distributions. The mean and standard deviation of the pdf will serve as the original 'parent' value for the evolutionary mutation sequence.

```matlab
function [pd_mean,pd_std] = CreateFit(emodulus,Printfn,fits)
%CREATEFIT    Create plot of datasets and fits

% figfunc=figure;
e=sort(emodulus);
e = e(:);
fits_str=num2str(fits);
mfd=6; %minimum number of fitted data
w=zeros(fits);
for i=1:fits
    w(i)=1/fits;
end

%%Prepare figure
 clf;
 hold on;
 LegHandles = []; LegText = {};
% --- Plot data originally in dataset "emodulus data"
 [CdfF,CdfX] = ecdf(e,'Function','cdf');    compute empirical cdf
 BinInfo.rule = 3;
 BinInfo.nbins = 50;
 [~,BinEdge] = internal.stats.histbins(e,[],[],BinInfo,CdfF,CdfX);
 [BinHeight,BinCenter] = ecdfhist(CdfF,CdfX,'edges',BinEdge);
 hLine = bar(BinCenter,BinHeight,'hist');
 set(hLine,'FaceColor',[.8 .8 .8],'EdgeColor','black',...
    'LineStyle','-', 'LineWidth',1);
 title('The Empirical Cumulative Distribution Function Histogram and the Fitted Probability Distribution Functions');
 xlabelText=('Elastic Modulus E [GPa]');
 xlabel(xlabelText);
 ylabel('Density')
 LegHandles(end+1) = hLine;
 LegText{end+1} = 'Empirical Cumulative Distribution Histogram';
```

```matlab
% Create grid where function will be computed
XLim = get(gca,'XLim');
XLim = XLim + [-1 1] * 0.01 * diff(XLim);
XGrid = linspace(0,XLim(2),100);

%% Creating estimated exclusion limits: the values where the fitted data is divided, where the new curve
begins.

e_min=min(e);
e_max=max(e);
place_e_min=find(e==e_min);
place_e_max=find(e==e_max);

% 1. we exclude the first smallest measured values, which have a  difference greater, than the interval
of the fits, as they obviously represent a measurement error

for i=2:length(e)
  if e(i)-e(i-1)>(e_max-e_min)/fits
    place_e_min=i;
    e_min=e(place_e_min);
  end
end

% 2. we make sure that the number of data to be fitted equals or is greater, than the minimum

if (place_e_max-place_e_min)/fits<mfd
    Message_mfd=('Not enough data for this number of fits!');
    Icon=('warn');
    h=msgbox(Message_mfd,Icon);
  end

% 3. Calculating the exclusion limits of the fitted intervals
if fits==1
    ex=1;
else
    ex=zeros(fits-1,1);
end
for i=1:(fits-1)
 ex(i)=(e_max-e_min)*i/fits+e_min;
```

```matlab
    end

    % Checking if Fit is possible on the interval: number of minimum fitted data is reached. If not, the limits
are moved.
  interval=zeros(fits,1);
 for i=1:fits
    if  i==1
        interval(i)=length(e(e >= e_min & e < ex(i)));
    elseif i==fits
        interval(i)=length(e(e > ex(i-1) & e <= e_max));
        ex(i)=e_max;
    else
        interval(i)=length(e(e > ex(i-1) & e < ex(i)));
    end
 end

if fits>1
    for i=1:fits
    k=1;
      while interval(i)<mfd
      %de1=0;
      %de2=0;
      lim_int_up=place_e_min-1;
      lim_int_low=place_e_min;
       for j=1:i
         lim_int_up=lim_int_up+interval(j);
         %de1=e(lim_int_up+1)-e(lim_int_up);
         if j==i
            break
         end
         lim_int_low=lim_int_low+interval(j);
         %de2=e(lim_int_low)-e(lim_int_low-1);
       end
       if i==1
          ex(i)=e(lim_int_up+1);
          interval(i)=interval(i)+1;
          interval(i+1)=interval(i+1)-1;
       end
       if i==fits
           ex(i-1)=e(lim_int_low-1);
```

```matlab
                    interval(i)=interval(i)+1;
                    interval(i-1)=interval(i-1)-1;
                end
            if i<fits %&& interval(i+1)>mfd+1 %&& de1<de2
                    ex(i)=e(lim_int_up+1);
                    interval(i)=interval(i)+1;
                    interval(i+1)=interval(i+1)-1;
                end
            k=k+1;
            if k==100
                    break
            end
        end
    end
end


%%Create fit

    pd_mean=zeros(1,fits);
    pd_std=zeros(1,fits);

if fits==1
    pd1 = fitdist(e, 'normal');
     YPlot = pdf(pd1,XGrid);
     hLine = plot(XGrid,YPlot,'Color','green',...
         'LineStyle','-', 'LineWidth',2,'Marker','none', 'MarkerSize',6);
    pd_mean(i)=mean(pd1);
    pd_std(i)=std(pd1);
else
   for i=1:fits
     if i==1
       Excluded = (e > e_min & e < ex(i));
     elseif i==fits
       Excluded = (e > ex(i-1) & e < e_max);
     else
       Excluded = (e > ex(i-1) & e < ex(i));
     end
       Data = e(Excluded);
       pd1 = fitdist(Data, 'normal');
       pd_mean(i)=mean(pd1);
```

```matlab
        pd_std(i)=std(pd1);
         YPlot = pdf(pd1,XGrid)*w(i);
         hLine = plot(XGrid,YPlot,'Color','green',...
            'LineStyle','-', 'LineWidth',2,...
            'Marker','none', 'MarkerSize',6);
     end
   end
       LegHandles(end+1) = hLine;
      LegText{end+1} = [fits_str,' initial Gaussian Probability Distribution Functions'];
   % Create legend from accumulated handles and labels
   hLegend = legend(LegHandles,LegText,'Orientation', 'vertical', 'Location', 'NorthWest');
   % Adjust figure
   box on;
   hold off;
   print(figfunc,'-dtiff',Printfn);
   savefig(Printfn);
   close(figfunc);
end
```

# Function "Mutate"

Function "Mutate" fits ncdf functions on the original data using evolutionary strategy.

```
function[ncdf_p,ncdf_p_fits,p_mean,p_std,w,ssr,r2]=Mutate(p_mean,p_std,w,e,f,sst,fits,c,d)
%Deifining variables
  p_mean_mut=zeros(1,fits);
  p_std_mut=zeros(1,fits);
  w_mut=zeros(1,fits);
  % (z,z_std,z_w: random parameters for max. 5000 mutations)
  z=normrnd(0,1,fits,5000);
  z_std=normrnd(0,1,fits,5000);
  z_w=rand(fits,5000);
  s_mean=(rand(1,fits))*c; % scattering for mean with ratio (c,d): weight scatter to mean and std scatter
  s_std=(rand(1,fits))*c; % scattering for std
  s_w=(rand(1,fits))*d; % scattering for w
  h=0.85; % stepsize
  k=0; % counter
  t=0; % counter w_mut
  tol=0.00009; %tolerance
  pm=ones(1,5000);
  RR=ones(1,5000);


 %%%%%% Mutation sequence


  for i=1:size(z,2)
    %mutation mean values & standard deviation=parent value+scatter*normal random
    for j=1:size(z,1)
    p_mean_mut(j)=p_mean(j)+(s_mean(j)*z(j,i));
    p_std_mut(j)=p_std(j)+(s_std(j)*z_std(j,i));
    end
    %mutation of weighting factor
    for j=1:size(z_w,1)
      w_mut(j)=w(j)+(s_w(j)*z_w(j,i));
    end
    while (sum(w_mut)~=1) % sum of w must be 1!
      w_mut=w_mut/sum(w_mut);
      t=t+1;
      if (t>1000)
        break;
```

```matlab
        end
    end

    ncdf_p_fits=zeros(size(e,1),fits);
    ncdf_p_mut_fits=zeros(size(e,1),fits);
    ncdf_p=zeros(size(e,1),1);
    ncdf_pmut=zeros(size(e,1),1);
    ncdf_wmut=zeros(size(e,1),1);
    ncdf_pmut_wmut=zeros(size(e,1),1);

    for j=1:fits
        ncdf_p_fits(:,j)=normcdf(e,p_mean(j),p_std(j)); % ncdf curves for all the fits
        ncdf_p_mut_fits(:,j)=normcdf(e,p_mean_mut(j),p_std_mut(j)); % mutated ncdf curves for all the fits
        ncdf_p=ncdf_p+ncdf_p_fits(:,j)*w(j); % 1. original distribution & original weighting
        ncdf_wmut=ncdf_wmut+ncdf_p_fits(:,j)*w_mut(j); % 2. calculating offspring with original
distribution & mutated weighting
        ncdf_pmut=ncdf_pmut+ncdf_p_mut_fits(:,j)*w(j); % 3. mutated distribution & original weighting
        ncdf_pmut_wmut=ncdf_pmut_wmut+ncdf_p_mut_fits(:,j)*w_mut(j); % 4. calculating offspring with
mutated distribution & mutated weighting
    end

    %calculating error for all combiniations
    e_ncdf_p=zeros(length(e));
    e_ncdf_wmut=zeros(length(e));
    e_ncdf_pmut=zeros(length(e));
    e_ncdf_pmut_wmut=zeros(length(e));

    for j=1:length(e)
        e_ncdf_p(j)=(ncdf_p(j)-f(j+1))^2;
        e_ncdf_wmut(j)=(ncdf_wmut(j)-f(j+1))^2;
        e_ncdf_pmut(j)=(ncdf_pmut(j)-f(j+1))^2;
        e_ncdf_pmut_wmut(j)=(ncdf_pmut_wmut(j)-f(j+1))^2;
    end

    error_ncdf_p=sum(e_ncdf_p(:));
    error_ncdf_wmut=sum(e_ncdf_wmut(:));
    error_ncdf_pmut=sum(e_ncdf_pmut(:));
    error_ncdf_pmut_wmut=sum(e_ncdf_pmut_wmut(:));

    err=[error_ncdf_p error_ncdf_wmut error_ncdf_pmut error_ncdf_pmut_wmut];
```

```matlab
% find minimum error to decide parents for next generation
if (min(err)==err(2))%p original w mutated
    w=w_mut;
    k=k+1;
end
if (min(err)==err(3))%p mutated w original
    p_mean=p_mean_mut;
    p_std=p_std_mut;
    k=k+1;
end
if(min(err)==err(4))%p mutated w mutated
    p_mean=p_mean_mut;
    p_std=p_std_mut;
    w=w_mut;
    k=k+1;
end


ifp=fits*3-1;
if (mod((i/ifp),10)==0) %ifp=number of independently fitted paramters
    if (k < (ifp*2)) % 1/5 success rule
        s_mean=s_mean/h; % adapt step size
        s_std=s_std/h; % adapt step size
        s_w=s_w/h;
    end
    if (k > (ifp*2))
        s_mean=s_mean*h;
        s_std=s_std*h; % adapt step size
        s_w=s_w*h; % adapt step size
    end
end
 if (mod((i/ifp),10)==0)
   k=0;   %reset counter
 end


 % if parameters are within the tolerance in the 1000 cycles
 ncdf_p=zeros(size(e,1),1);
 ncdf_p_fits=zeros(size(e,1),fits);
```

```matlab
        for j=1:fits
            ncdf_p_fits(:,j)=normcdf(e,p_mean(j),p_std(j));
            ncdf_p=ncdf_p+ncdf_p_fits(:,j)*w(j);
        end
    ssr=sum((f(2:end)-ncdf_p').^2);
    r2=1-(ssr/sst);
    pm(i)=r2;


    %relative error within the mutation cycle
        E_max=max(e);
        E_min=min(e);
        Integral_ncdf=trapz(ncdf_p,e);
        Integral_ecdf=trapz(f(2:end),e);
    rel_err(i)=abs(Integral_ncdf-Integral_ecdf)/(E_max-E_min)*100;


    if (i>1000)
        con=abs(pm(i)-(mean(pm(i-1000):pm(i))));
        if con<tol
        break;
        end
    end
end % end of mutation sequence


%%%Print the evolution of R2 and relative error within the mutation cycle
 fig=figure;
 hold on;
 grid on;
 ix=[1:1:i];
 [AX,PM,RR]=plotyy(ix,pm(1,1:i),ix,rel_err(1,1:i));
   set(get(AX(1),'Ylabel'),'String','Coefficient of determination')
   set(get(AX(2),'Ylabel'),'String','Relative error [%]')
   xlabel('Mutation cycles')
   title('Development of R2 and relative error within the evoltution process')
   legend('R^2','Relative error')
   fits_str=num2str(fits);
box on;
hold off;
 print(fig,'-dtiff',['plotyy',fits_str,'.tiff']);
 close(fig);
```

# Function "Printfit"

Function "Printfit" plots the original data as histogram and the fitted probability distribution functions as curves.

```matlab
function [Fit]=PrintFit(emodulus,p_mean,p_std,w,Printfn,fits)

figfunc=figure;
emodulus = emodulus(:);

%%% Prepare figure
clf;
hold on;
LegHandles = []; LegText = {};

% --- Plot data originally in dataset "emodulus data"

[CdfF,CdfX] = ecdf(emodulus,'Function','cdf');  % compute empirical cdf
BinInfo.rule = 3;
BinInfo.nbins = 50;
[~,BinEdge] = internal.stats.histbins(emodulus,[],[],BinInfo,CdfF,CdfX);
[BinHeight,BinCenter] = ecdfhist(CdfF,CdfX,'edges',BinEdge);
hLine = bar(BinCenter,BinHeight,'hist');
set(hLine,'FaceColor',[.8 .8 .8],'EdgeColor','black',...
    'LineStyle','-', 'LineWidth',1);
title('The Empirical Cumulative Distribution Function Histogram and the Mutated Probability Distribution Functions');
xlabel('Elastic Modulus E [GPa]');
ylabel('Density')
LegHandles(end+1) = hLine;
LegText{end+1} = 'Empirical Cumulative Distribution Histogram';

% Create grid where function will be computed
XLim = get(gca,'XLim');
XLim = XLim + [-1 1] * 0.01 * diff(XLim);
XGrid = linspace(0,XLim(2),100);

% --- Create fit
SumFit=0;
for i=1:fits
```

```matlab
    fits_str=num2str(i);
  Fit= ProbDistUnivParam('normal',[ p_mean(i), p_std(i)]);
  YPlot = pdf(Fit,XGrid)*w(i);
 if i==fits
    hLine = plot(XGrid,YPlot,'Color','red',...
       'LineStyle','-', 'LineWidth',3,...
       'Marker','none', 'MarkerSize',6);
       LegHandles(end+1) = hLine;
       LegText{end+1} = ['Theoretical distribution number ',fits_str,' - intact phase'];
  else
    hLine_blue = plot(XGrid,YPlot,'--rs','Color','blue',...
       'LineWidth',1,...
       'Marker','none', 'MarkerSize',6);
  end
  SumFit=SumFit+YPlot;
end
    if i~=1
       LegHandles(end+1) = hLine_blue;
       LegText{end+1} = ['Theoretical distributions - damaged material phases'];
    end
       hLine = plot(XGrid,SumFit,'Color','k',...
       'LineStyle','-', 'LineWidth',1,...
       'Marker','none', 'MarkerSize',6);
       LegHandles(end+1) = hLine;
       LegText{end+1} = ['Sum of ',fits_str,' theoretical distributions'];


% Adjust figure
grid on;
box on;
hold off;

% Create legend from accumulated handles and labels
hLegend = legend(LegHandles,LegText,'Orientation', 'vertical', 'Location', 'NorthWest');
set(hLegend,'Interpreter','none');
print(figfunc,'-dtiff',Printfn);
fits_str=num2str(fits);
Printfn=['Sample_all_fitted_pd_',fits_str,'.fig'];
close(figfunc);
```

*Published with MATLAB® R2012b*

# References

Jaindl, M., Reinbacher-Köstinger, A., Magele, C., Renhart, W., Multi-objective optimization using evolution strategies, Electron. Energetics 22 (2) (2009) 159–174.

Kariem, H., Pastrama M.-I., Roohani-Esfahani, S.I., Pivonka, P., Zreiqat, H., Hellmich C., 2015. Micro-poro-elasticity of baghdadite-based bone tissue engineering. Mat. Sci. Eng., 553-564.

Lucchini, R., Carnelli, D., Ponzoni, M., Bertarelli, E., Gastaldi, D., Vena, P., 2011. Role of damage mechanics in nanoindentation of lamellar bone at multiple sizes: Experiments and numerical modeling. J. Mech. Beh. Biomed. Mat. 4 (8), 1852-63.

Luczynski, K.W., Steiger-Thirsfeld, A., Bernardi, J., Eberhardsteiner, J., Hellmich, C., 2015. Extracellular bone matrix exhibits hardening elastoplasticity and more than double cortical strength: Evidence from homogeneous compression of non-tapered single micron-sized pillars welded to a rigid substrate. J. Mech. Beh. Biomed. Mat., In Press, Corrected Proof.

Schwaiger, C., 2014. Bone elasticity determination: quasi-static unloading tests, ultrasound, and micromechanics. Master's Thesis, Vienna University of Technology (TU Wien).

Weicker, K., 2007. Evolutionäre Algorithmen. Leitfäden der Informatik, Vieweg+TeubnerVerlag.